ACS APPLIED MATERIALS & INTERFACES

Review

www.acsami.org

Joining of Silver Nanomaterials at Low Temperatures: Processes, Properties, and Applications

Peng Peng,*[,†,‡] Anming Hu,[§] Adrian P. Gerlich,[†] Guisheng Zou,[∥] Lei Liu,[∥] and Y. Norman Zhou*[,†,‡,∥]

[†]Centre for Advanced Materials Joining and [‡]Waterloo Institute for Nanotechnology, University of Waterloo, 200 University Avenue West, Waterloo, ON N2L 3G1, Canada

[§]Mechanical, Aerospace and Biomedical Engineering Department, University of Tennessee, 1512 Middle Drive, Knoxville, Tennessee 37996-2210, United States

[∥]Department of Mechanical Engineering, Tsinghua University, Beijing, 100084, China

ABSTRACT: A review is provided, which first considers low-temperature diffusion bonding with silver nanomaterials as filler materials via thermal sintering for microelectronic applications, and then other recent innovations in low-temperature joining are discussed. The theoretical background and transition of applications from micro to nanoparticle (NP) pastes based on joining using silver filler materials and nanojoining mechanisms are elucidated. The mechanical and electrical properties of sintered silver nanomaterial joints at low temperatures are discussed in terms of the key influencing factors, such as porosity and coverage of substrates, parameters for the sintering processes, and the size and shape of nanomaterials. Further, the use of sintered silver nanomaterials for printable electronics and as robust surface-enhanced Raman spectroscopy substrates by exploiting their optical properties is also considered. Other low-temperature nanojoining strategies such as optical welding of silver nanowires (NWs) through a plasmonic heating effect by visible light irradiation, ultrafast laser nanojoining, and ion-activated joining of silver NPs using ionic solvents are also summarized. In addition, pressure-driven joining of silver NWs with large plastic deformation and self-joining of gold or silver NWs via oriented attachment of clean and activated surfaces are summarized. Finally, at the end of this review, the future outlook for joining applications with silver nanomaterials is explored.

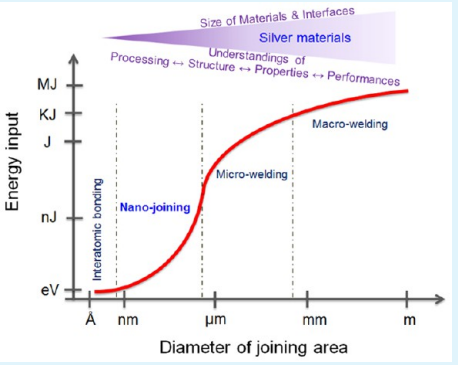

KEYWORDS: *review on nanojoining, low temperature, silver nanomaterials, size effects, mechanical properties*

1. INTRODUCTION

Nanostructured noble metallic materials, in particular, silver, are widely studied because of their excellent combination of optical properties and electrical and thermal conductivities compared to other metals. Nowadays, the synthesis of various silver nanomaterials, including zero-dimensional nanocubes, nanodecahedrons, nanospheres, nanoplates, nanodisks, and one-dimensional silver nanowire (NW), nanobelts, and nanotubes have been well-developed.[1−7] To utilize such shaped nanomaterials for functional devices, joining of those nanoscale building blocks is essential to any manufacturing processes. However, producing permanent connections among such nanosized structures and forming nanosystems, and then integrating these connected materials into bulk components or their surroundings, remains a challenge.[8]

At the macro and micro scales, various joining processes have been developed to fabricate metallic interconnects for achieving good mechanical strength and electrical conductivity in bulk materials. Roughly, they can be classified into three major types based on the physical states of the parts to be joined: fusion welding, soldering/brazing, and solid-state bonding.[9] In general, fusion welding processes involve high local heat input and high temperatures using various energy sources, including laser,[10−12] electron beam,[13] electrical resistance,[14] plasma,[15] microwave,[16−18] and chemical reaction,[19] to cause local melting and coalescence of the base building blocks. In terms of soldering and brazing, important methods of joining materials without melting the base components, molten filler metal is introduced between the base components producing a metallurgical reaction, which includes the dissolution process of the solid base metal into molten liquid and then formation of a reaction layer between them.[8,20] Among brazing and soldering, the filler metals having low liquidus temperatures (<450 °C) are used during soldering as a widely used microjoining technique in electronic packaging industry, and the solder may contain lead, which has raised much concern due to health, environmental, and safety issues worldwide. Presently, even the well-developed lead-free soldering technology,[21−24] where the general melting point of filler metals ranges from 200 to 300 °C, is still inadequate to satisfy the requirement of interconnection of heat-sensitive substrates, thus restricting the popularization of flexible electronic or organic light-emitting devices,[25−27] and ferroelectric materials with low transition temperature or organic ferroelectric

Received: March 10, 2015
Accepted: May 25, 2015
Published: May 25, 2015

DOI: 10.1021/acsami.5b02134
ACS Appl. Mater. Interfaces 2015, 7, 12597−12618

materials.[28−30] Solid-state bonding processes, such as friction welding,[31,32] cold (pressure) welding, diffusion welding, or ultrasonic wire bonding,[33] introduce high strain and plastic deformation to the parts at elevated temperatures. Solid-state sintering, or even diffusion bonding of bulk materials, are typically performed in an inert atmosphere or vacuum and involve temperatures of at least half of the melting point, with pressures between 1 to 10 MPa.[34] The bond formation generally takes place in two steps, first where a partial bond is formed and the asperities between the components begin to collapse with residual porosity between the joined asperities. Then a more complete bond is formed after prolonged times at high temperatures such that diffusion and creep increase the contact area.

It is well-known that, as the size range transitions to the nanoscale, higher specific surface energy and increasing surface-to-volume ratio in the nanostructured materials enhances their sensitivity to heat.[35] Although laser welding,[10−12] resistance spot-welding,[36] ultrasonic bonding,[37] and soldering[14,38,39] have been applied on nanomaterials successfully as in the case of welding of bulk materials, these conventional methods with high heat input risk damage to the ever-smaller and more delicate microelectronic components and/or nano-objects when their original shapes and structures must be maintained. Therefore, a low-temperature or even room-temperature interconnecting technique, such as optical welding[40] or cold welding,[26,41] is required to minimize the heat effects on the properties of heat-sensitive components during assembly.

Some studies have been focused on interconnecting individual silver nanomaterials to explore their application in nanodevices.[42] Since the contact interface is at a nanoscale for interconnecting nanomaterials, little energy input is required to achieve metallic bonding via interdiffusion compared to macroscale joining, suggesting that the joining processes at nanoscale might be able to proceed at low temperatures. Some approaches have been shown to benefit from nanotechnology, in which nanoscale diffusion bonding using metallic nanomaterials offers significant advantages over conventional soldering or adhesive bonding, such as lower bonding temperatures and higher diffusion rates.[8] It is worth noting that this size effect has been long proposed as a fundamental thermodynamic factor that suppresses the melting point of metals at a nanoscale.[43,44] Considering the size effect and nanoscopic diffusion process of nanomaterials, developing a bonding method that can work at low temperatures by using silver nanomaterials is important for polymer and flexible electronics. Recently, the low-temperature joining technology developed using metallic nanoparticle (NP) pastes, such as silver,[45−49] copper,[50−52] gold,[53] and silver−nickel,[54] appears to be a promising alternative for lead-free electronic packaging and flexible electronic interconnections.

To-date, various nanosilver pastes have been used to bond bulk components for electronic packaging, providing novel mechanical and electrical properties, and as optical substrates for biosensing with their tunable optical properties. The mechanical properties of sintered silver NP joints have been reviewed in detail by Siow from the point view of die attachment materials.[55] Thermal sintering is the main mechanism involved in forming silver NP joints for low-temperature diffusion bonding. However, other physical properties of these sintered nanomaterials and relative applications have received little attention. Herein, this review is designed to cover thermal-mechanical, mechanical, electrical, and optical properties of sintered silver nanomaterials and their emergent applications. Beyond conventional thermal sintering at elevated temperatures, recent developments in low-temperature sintering to interconnect silver nanomaterials also merit a review in terms of the history of silver based pastes and sintering concepts at the micro- and nanoscales. The mechanical properties of sintered nanomaterial joints and the parameters for improving their strength are also summarized in this review, along with the measured electrical conductivity and electromigration properties of sintered nanomaterials. Further, sintered silver nanomaterials have been considered for new biodetection applications considering their optical properties. In the second portion of this review, recent advances in other low-temperature joining methods, such as optical welding, pressure joining, chemically activated sintering, and self-joining are reviewed in a broader scope. The joining mechanisms and future developments of such strategies are elucidated. This article is intended to be a useful primer for researchers who are exploring nanopastes as options for lead-free soldering materials, for interconnection of nanomaterials at low temperatures or even room temperature, and for developing other new applications.

2. OVERVIEW OF NANOJOINING

2.1. Basic Concepts. A joining process leads to formation of permanent connections between building blocks with primary (and occasionally secondary) chemical bonds between faying surfaces.[8] For the case of silver nanomaterials, metallurgical bonding is primarily required. In principle, when two perfectly clean and flat solid surfaces are close enough, they will form bonds together spontaneously through interatomic forces. In practice, most material surfaces are not ideal. The unavoidable roughness and contamination on the surfaces will create obstacles for joining. To overcome these surface impediments for a joint, some form of energy, for example, heat and/or pressure, is required.[8] At a nanoscale, these impediments on the surfaces could be dramatically minimized due to the much-reduced surface areas and lower chances to encounter defects. Therefore, joining at a nanoscale, the so-called nanojoining process will require lower energy per unit surface area than that of micro- and/or macroscale joining. Also, the changes of physical or chemical properties of materials at a nanoscale and the manipulation processes at such scale play essential roles for joining.

2.2. Size Effects on Melting and Sintering Temperatures. Joining occurs by migration of atoms mainly along the particle surfaces, suggesting that surface energy and curvature would be the dominant factors for joining. Surface energy γ is an excess free energy, and it is the reduction in surface area that drives the joining process. It is defined to be the energy to create a unit area of surface.[56]

The driving force at the interface when two spherical particles contact is given by the Laplace equation

$$P = P_0 + \gamma\left(\frac{1}{R_1} + \frac{1}{R_2}\right) \quad (1)$$

where R_1 and R_2 are the principal radii of curvature at the contact point of the surface. P_0 is the pressure external to the surface, and γ is the surface energy, $\gamma = ((\partial G)/(\partial A))_{T,P,n}$. The surface energy includes the structural contribution due to surface stress derivation and surface chemical contribution from the energy in breaking bonds related not only to curvature, but also to stress and composition.[57] Therefore, the driving force

DOI: 10.1021/acsami.5b02134
ACS Appl. Mater. Interfaces 2015, 7, 12597−12618

for reduction of surface area will increase when the size of particles decreases to nanoscale.

Generally, in the case of sintering, the sintering process is controlled by sintering temperature and time. The sintering temperatures of materials can be written as

$$T_s = \alpha T_m \tag{2}$$

where T_s is the sintering temperature, and T_m is melting temperature dependent on the material. Factor α is relative to material geometries and other environmental conditions. Thus, the effective sintering temperature is contributed by two aspects, namely, coefficient α and melting temperature T_m. Although sintering processes proceed without melting in most cases, the decrease of T_m in NPs can contribute to the decreasing of sintering temperature compared with bulk sintering. On the basis of modified versions of the Debye model for size dependence of melting point,[58,59] it can be shown that the sintering of NPs is enhanced by the suppression of the melting point T_m, which is reduced from that of the bulk material melting point (T_{mb}) by a factor as follows:[60,61]

$$T_m = T_{mb}\left(1 - \frac{\delta}{D}\right) \tag{3}$$

where D is the particle diameter, and δ is a material-dependent parameter with reported values from ~1.80 to 2.65 nm for various metals,[44] depending on the atomic volume and solid−vapor interfacial energy[61] (related to the bonding energy of the crystal structure). Thereby, the fact that $T_m < T_{mb}$ for NPs contributes to a reduced sintering temperature. The other influence factor α is usually selected to be 0.8 for bulk materials[62] ($T_s = 0.8T_{mb}$). However, the sintering of microparticles can proceed at $0.5-0.8T_m$,[63−65] while values of $0.1-0.3T_m$[63,66] have been reported for NPs, and Monte Carlo and molecular dynamic simulations show even lower temperatures down to a few Kelvins.[67−69] The reduction of the influence factor from 0.8 to 0.3 is attributed to the larger driving force for NPs as previously mentioned and further reduces the joining temperatures.

2.3. Nanojoining Mechanisms. As discussed above, due to size effects, a nanomaterial will be more active during joining because of the lower melting points and larger portions of atoms on the surface than bulk materials (see Figure 1a). These will lead to a more surface-dominated process when joining two NPs. If the thickness of the joining area reduces to a couple of nanometers (a few atomic layers), then interatomic forces will facilitate the formation of primary bonds. Thus, interatomic bond intensity is in a range of a few electronvolts to nanojoules; see Figure 1b. In the nanojoining regime, surface impediments (roughness or contamination) are insignificant and negligible in some cases, and the surface diffusion will facilitate the joint associated with very limited external energy. As the size scale is further extended into the microwelding regime, remarkable energy is required to overcome the surface impediments. In addition, the energy could not be precisely delivered onto the surface (or location) required for joining due to the limitation of current techniques, and most applied energy will be dissipated elsewhere around the joint and lead to more bulk heating during joining. This suggests a correlation between the energy input requirements and joining area.

Generally speaking, a nanoscopic interconnection will require very limited energy since the diffusion of surface atoms is driven by a high surface energy. Nanojoining may even occur by surface diffusion without external energy as a trigger.

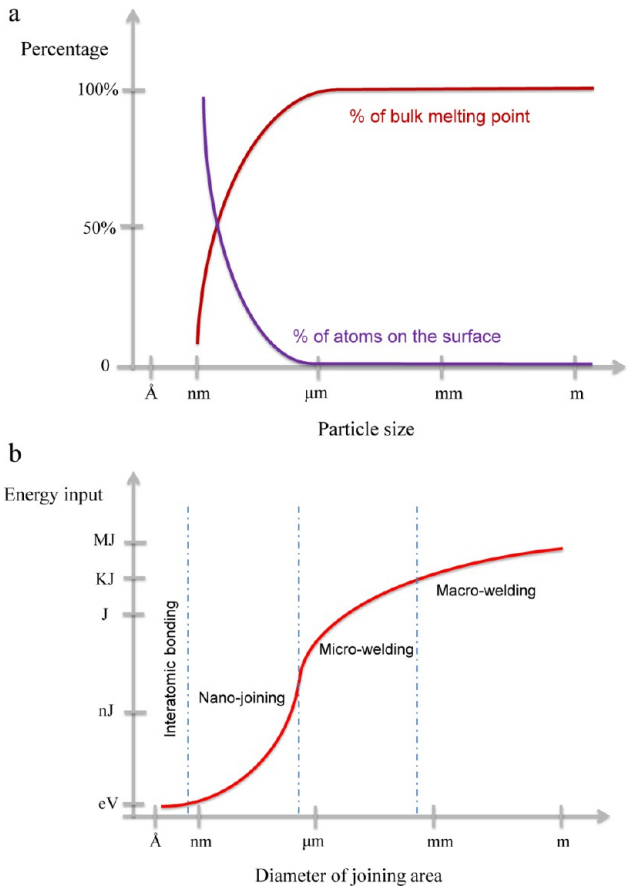

Figure 1. (a) General trend of melting point and percentage of atoms on surface of particles. (b) Energy input for joining (assuming joining time is ~1s).

Taking sintering as the joining case, the joining process begins with rapid neck formation followed by neck growth initially by surface diffusion and then by vapor condensation. Surface and grain-boundary diffusion are the two main mechanisms throughout the entire joining process, although dislocations are present at the early stage of the joining. Grain-boundary diffusion promotes the neck size growth[70] as illustrated in the numerical modeling results in Figure 2. Faster surface diffusion plus evaporation condensation at higher temperatures are also among the factors promoting faster neck size growth.

Currently, the sintering behaviors among individual spherical particles have been well-established.[71−75] However, materials with different shapes are rarely considered in studies of sintering behaviors. The above model only describes the sintering behaviors between spherical particles. Since other shaped materials, such as fibers, belts, and disks,[69] are different from the spherical case, it may not be suitable for them. Therefore, starting from a small scale, the study of nanosintering processes of different shaped nanomaterials could enrich the sintering theory. The joining mechanisms among other nanojoining processes also need to be studied. From the particle size point of view, the effect of reduction from micro- to nanoscale particles has begun to be studied and draws considerable attention. This transition will be discussed in the next section.

2.4. From Silver Micro- to Nanosintering. Since the late 1980's, electronics packaging has employed Ag material pastes

DOI: 10.1021/acsami.5b02134
ACS Appl. Mater. Interfaces 2015, 7, 12597−12618

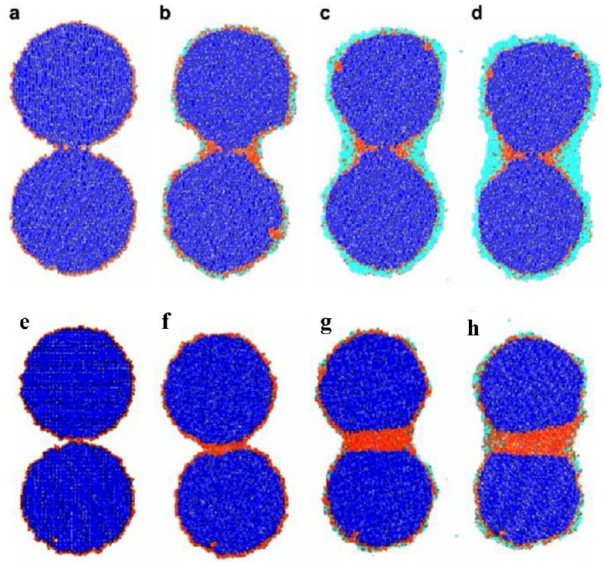

Figure 2. Molecular dynamics simulation of two large particles sintering at $T = 63\%\ T_m$. (a–d) without grain boundary and (e–h) with grain boundary. Snapshots for the sintering process are t = 500, 50 000, 200 000, and 500 000 steps. Every particle contains ~3000 atoms with bulk atoms (blue), surface or grain-boundary atoms (red), and vapor-state atoms (cyan), respectively. Reprinted with permission from ref 70. Copyright 2009 Elsevier.

as a die attach material.[76] Usually, the weight percentage of the metallic particles in the paste has been ~70–80%.[77] The rest is composed of organic solvents, dispersants, and polymer-based binders to increase the material stability and processability. The rheology of the paste can be tuned by using different surfactants and particle sizes.[78−81] Binders and dispersants serve the same function of dispersing the particles, and both terms have been often used interchangeably in literature.[55] These can prevent agglomeration of particles in the paste but will also hamper the sintering process. Therefore, the reduction of such organics can achieve lower sintering temperatures.[82] Elevated temperatures are usually used to remove the organics during the bonding process. Their release can generate voids after sintering as well. Generally, sintering pressure, time, temperature, particle size, and the surface condition of substrates could influence the joint properties significantly. However, large pressures, typically above 10 MPa,[76] could be needed to achieve robust bonding, which may be unsuitable for practical applications. Hence, various research efforts have been conducted to reduce the sintering pressure during bonding processes.

It has been found that the surface diffusion coefficient increases with the decrease of NP size suggesting a higher specific surface energy of NPs than that of the microparticles or bulk materials. Considering that the driving force for diffusion is inversely proportional to the size of the particles as mentioned in Section 2.2, a high driving force results in a decrease in sintering temperature of NPs.[83] The suppression of melting temperature (as shown in eq 3) and the presence of a surface premelting layer (as observed with molecular dynamic simulation[61,84]) will enhance the sintering of NPs. It also appears that smaller NPs could be interconnected under lower external pressure since the stresses at contact areas increase with reducing NP size. Therefore, replacing microflakes with NPs will simultaneously induce low sintering temperatures and required pressure, making low-temperature joining feasible. For example, these factors may make it possible for significant sintering to occur at less than one-third of the melting temperature of the materials, a temperature where traditional diffusion bonding of bulk materials is not normally feasible.[63] Table 1 summarizes the most-used metal nanomaterials to replace Ag microflakes for electronic packaging. They can be categorized into a few groups: noble metal NPs and their mixture, metal oxide NPs, tin-based alloy NPs, noble metal NPs with tin alloy NPs. Ag NP-based pastes are the most developed one at this moment. Aside from thermal sintering, pulsed electric current sintering has also been employed to join Ag NPs.[85,86] Meanwhile, some attention has been drawn to the mixture of a few different metal NPs with additions of metal oxide NPs or alloy NPs. In the next section, only Ag nanomaterials as filler materials for joining will be discussed.

3. MICROSTRUCTURES AND MECHANICAL PROPERTIES OF SILVER JOINTS VIA NANOSINTERING

3.1. Porosity and Coverage. Currently, the leading application for sintered nanomaterial joints is for microelectronic packaging.[113] Figure 3 shows a schematic of nanomaterials being used as filler materials to bond two components together. For example, this would be the typical case where a Ag-based nanopaste, containing Ag NPs and organic binders, is uniformly coated on clean surfaces of two bulk components. The components are typically held under a low compressive stress with the Ag nanopastes at the interface and sintered at a specific time and temperature; see Figure 3a. Often a shielding gas or vacuum is needed in the sintering processing to suppress oxide formation with more reactive nanomaterials. The bonded joints can be evaluated in terms of their thermal, mechanical, and electrical properties, which will be reviewed later. Similarly, these properties are controlled by two interfaces: nanomaterials–nanomaterials and nanomaterials–substrates, as indicated in Figure 3b,c. It is worth noting that the bonding interface is built via a bottom-up approach, where the porosity of the sintered nanomaterials and substrate coverage need to be considered when discussing the mechanical and electrical properties. Some porosity of the sintered nanomaterials always remains since pathways for the release of organic binders and solvents will be required during sintering. To reduce the porosity, applying external pressure and presintering may be adopted, and these treatments can have a significant positive effect on joint properties. However, the pores at the interface of nanomaterials and substrates, referred to as coverage in the two-dimensional model shown in Figure 3c, are difficult to eliminate. Theoretically, there is only one layer of nanomaterials directly in contact with the substrates. Consequently, the coverage is $(1 - x/y)$, where x is the uncovered length, and y stands for the central distance of two NPs. To increase the coverage, the gap x should be decreased. Simply applying a force in one direction (vertically between two bulk components) cannot efficiently achieve a dense interface. Meanwhile, applying a force parallel to this interface (horizontally on the nanomaterials) is very difficult in practical applications since this filler layer is only tens of nanometers depending on the particle size in nanopastes.

3.2. Thermal-Mechanical Stabilities. The thermal reliability of power electronics is one important aspect when sintered silver nanomaterials were used as interconnection materials.[99,114−119] Ratcheting and creep behaviors of sintered joints have been studied at various temperatures and

DOI: 10.1021/acsami.5b02134
ACS Appl. Mater. Interfaces 2015, 7, 12597−12618

Publication Date (Web): June 4, 2015 | doi: 10.1021/acsami.5b02134

Table 1. Few Developed Metal Nanomaterials for Electronic Packaging Application in Recent Years

metal nanomaterials				sintering parameters						
element	shape	size (nm)	bonding substrates	temperature (°C)	time (min)	pressure (MPa)	atmosphere	properties	note	ref
Ag	NPs	3−20	Cu to Cu disc	300	5	1, 5	air	strength		Ide[87]
	NPs	50	Cu wire to Cu foil	140−300	30	5	air	strength		Alarifi[45]
			Cu wire to Au coated PI	100−250						Hu[88]
	NPs		Si/SiC to Cu or DBC	300	10−90	0	air	strength, thermal properties		Bai[46,89,90]
	NPs	20, 40, 90	Ag-coated Cu disc	250	30	5	air	strength	<100 °C drying	Yan[91−93]
		40						strength, wetting		
				160−350	5, 30	0, 5		strength	coffee ring effect	
		45, 40		250	30	5				
	NPs		device die-attach to DBC	240	5	40		strength, electrical resistivity, thermal conductivity	270 °C preheating	Zhang[94]
	NPs		Ti/Pd/Ag-coated AlN ceramics to Ag strip	250−270		5.5		thermal cycling resistance		Kähler[47]
	NPs	5, 10, 100	Cu to Cu disc	250	3	1−10	air	strength	100 °C and 60 min vacuum drying	Morita[95]
	NPs	13	Ag-coated Cu sheets	150−280	0.5−20	0	air	strength, conductivity	NP twinning effect	Wang[96]
	NPs		Ag-coated Cu plates	275	20	0−5	air	strength	multiple preheatings	Lei[97]
	NPs	<50	Cu dummy chip to DBC	275		5	vacuum	strength, thermal aging		Egelkraut[98]
	NPs	<50	die-attach to Ag-coated Cu	200−300	5s-30 min	0−30	air	density, strength, reliability	125 °C and 30 min predrying	Knoerr[99,100]
	NPs	20−168	Cu to Cu disc	250−350	5	0	air	strength		Morisada[101]
	Ag_2O NPs	<5 μm	Cu/Au-to-Cu/Au	140−400	1−5	5	air	strength	in situ Ag NPs by Ag_2O	Hirose[102]
	Ag_2O NPs		Si chip to Ag-coated Cu−Si_3N_4 substrate	300	10	0.3	air	reliability in power cycling test	40 °C and 10 min drying	Yasuda[103]
	Ag_2O NPs		Cu to Cu plates	2200 A and 99 ms		5	air	strength	Ag_2O for spot-welding	Suzuki[104]
	flakes	80 nm thick (8 μm diameter)	Si/SiC to DBC	300	60	0.4	air			Sakamoto[105]
	NP+NW	NP 50−100	Cu wire to Cu wire	60−200	60	0	air	strength		Peng[82,106]
	NWs	NW: 8−15 μm by50−100 nm		18−400		0		strength, resistivity		
	NP	20	CNTs-Si to Cu substrates with ECA (Ag filler)	150	90	0	air	I−V	CNT film transfer via conductive adhesive	Jiang[107]
Ag−Cu	mixed NP	Cu <200	Cu wire to Cu pad	100−200	30	10	air	strength		Yan[108]
		Ag < 100								
	mixed NPs	Cu:498	Cu to Cu disc	250−350	5	10	air	strength		Morisada[77]
		Ag:7.9								
	Cu@Ag core−shell	Core:470		220	10	0	Ar	thermal dynamics surface diffusion	78 MPa and 30 s prepressing	Kim[109]
		Shell:7								
Cu	NPs	20−110	Cu wire to Cu pad	110−280	30	5	air	strength, resistivity	80 °C preheating	Yan[50]

ACS Appl. Mater. Interfaces 2015, 7, 12597−12618 DOI: 10.1021/acsami.5b02134

Table 1. continued

metal nanomaterials			bonding substrates	sintering parameters			properties	note	ref
element	shape	size (nm)		temperature (°C)	time (min)	pressure (MPa)	atmosphere			
Cu-NiO	mixed NPs	Cu:230	Ni-coated Cu plates	350	5	0	H_2	strength	NiO-CuO solid solution to NiCu alloy	Satoh[110]
		NiO:50								
Au	NPs	2	Au-coated SiO_2 substrate	120–300	5–60	0	air	resistivity electromigration		Bakhishev[53]
Sn alloy	Sn NPs	26–85	On Cu substrate	220–230	5	0	air	solderability, wetting, melting, conductivity		Jiang[107]
	SnIn NPs	10–70								
	SnAg NPs	10–64								
	SnAgCu NPs	10–20								
	Sn, In mixed NPs	30–80	On Si	116, 136, 150	5–35		N_2	thermal properties, phase	preheating with soak, reflow in flux	Shu[111]
Cu–Ni_3Sn_2	Cu NPs	200	Cu to Cu plates	300–400	5	0	H_2	strength		Watanabe[112]
	Ni_3Sn_2 cube	8–15								

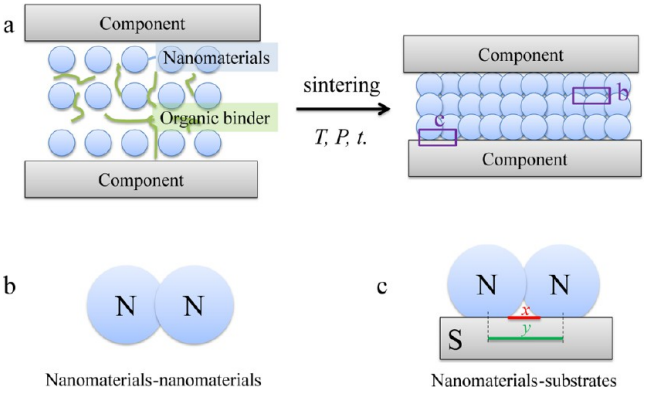

Figure 3. (a) Schematic of bonding with sintered nanomaterial fillers; *T*, *P*, and *t* stand for sintering temperature, pressure, and time, respectively. Interface qualities of nanomaterials–nanomaterials (b) and nanomaterials–substrates (c) affecting the joint properties.

stresses.[120−124] In this section, we mainly consider two kinds of thermal-mechanical properties, namely, thermal stability and thermal cyclic fatigue, of sintered nanomaterial joints. Unlike the typical solders, such as Sn–Ag–Cu, sintered nanomaterials will benefit from an enhanced sintering of the interconnections at higher temperatures suggesting they can survive when the temperatures go beyond the bonding temperature. In contrast, solder joints will melt and fail under higher temperatures. This suggests that sintered nanomaterial joints will survive longer and continue to function at higher temperatures[88,125] compared with the Sn solder joints, which is very important for practical applications especially when unexpected overheating occurs during device operation. Figure 4 illustrates the comparison of

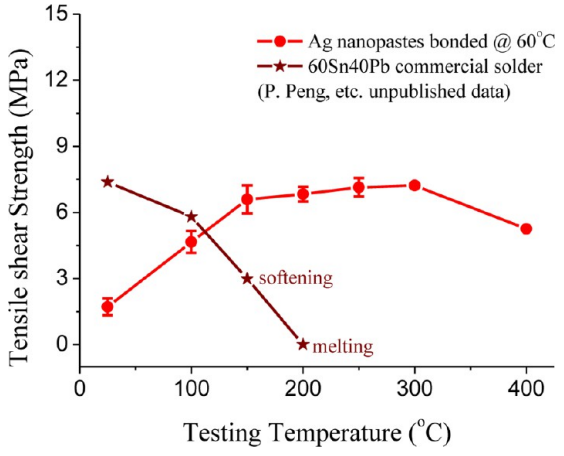

Figure 4. Comparison of joint strength using Ag NP paste and commercial Sn–Pb alloy.

the strength of joints with two kinds of filler materials, Ag NP and Sn–Pb alloy, tested at different temperatures. Obviously, Sn–Pb alloy will soften at 150 °C and melt at 200 °C, which could cause the failure of joints. However, the strength of sintered nanomaterial joints increased when testing temperature increased from room temperature to 300 °C. They did not fail even at temperatures beyond 300 °C, suggesting that sintered nanomaterial joints have better thermal stability than that of commercial Sn–Pb solders.

Lifetime in different thermal shock tests has been conducted on sintered joints utilizing nanoscale joining materials.[126] In the

DOI: 10.1021/acsami.5b02134
ACS Appl. Mater. Interfaces 2015, 7, 12597−12618

application of die attachment, tests were run to over 5000 thermal cycles (50 to 250 °C).[89,90] In Bai's study, the failure criterion was considered as a 50% drop in strength.[90] After 4000 cycles, the silver-coated substrates failed, while gold-coated substrates endured 6000 cycles. When the microstructure of these sintered nanomaterials was compared after different thermal cycles, significant microvoids were observed after 4000 cycles, which likely contributed to the degradation of strength. It can be expected that the sintered nanomaterials will coarsen after undergoing long sintering time at 250 °C, also leading to growth of pores. In another study, sintered nanomaterial joints with passive dies indicated no significant changes in the microstructure, and cracks appeared at a relatively low life of 800 cycles and lower temperatures (−40 to 125 °C).[127] The good thermal fatigue properties were enhanced by the absorption of thermal stresses by the porous sintered nanomaterials via plastic deformation.[55,127] In addition, a few reports have compared the durability of sintered nanomaterial joints with typically processed Sn solder joints, showing that the former have much better performance in thermal cycling applications.[48,99,128]

3.3. Processing Parameters for Enhanced Mechanical Properties. The mechanical properties of sintered nanomaterial joints can be affected by various parameters during the bonding process, including temperature, time, pressure, and the qualities of nanopastes (such as organic content in the paste and size and shape of nanomaterials). Since the strength discussed in published papers has involved pure tensile,[102] shear,[129] and a hybrid mode—tensile shear strength,[88] the testing mode was not strictly distinguished, but rather the term "strength" is used here instead to compare the values. Detailed discussion on all aspects of strength and elastic modulus can be found in Siow's recent review on mechanical properties of nanosilver joints.[55]

Usually, appropriate sintering temperatures are chosen according to the application requirement, substrates used, and the sinterability of pastes. These factors depend on the types and content of organic binders and dispersant in the pastes,[130,131] the different materials coated onto substrates, and the materials of substrates[132] (such as Ag/Au/Ni-coated Cu, bare Cu, or Ag/Au-coated plastics[45,46,82,87,88,93,102]). In this review, the strength information for bonded joints are all based on Cu substrates, which are mainly bare Cu or Ag-coated Cu.

3.3.1. Temperature. The elevated sintering temperature can produce higher strength of sintered nanomaterial joints due to more intense sintering between nanomaterials and nanomaterial to substrates. During initial development of low-temperature joining technology, the sintering temperatures ranged from 250 to 350 °C since a significant amount of polymers were added into the pastes to improve the stability of nanopastes and coating properties on substrates. Sintering temperatures have subsequently been reduced to below 200 °C successfully after many efforts, as shown in Figure 5. For example, poly(vinylpyrrolidone) (PVP)-coated Cu NPs were introduced into the paste to replace Ag NPs and achieved bonding at 170 °C.[50] An in situ transformed Ag NP from the Ag_2O method has been invented by Hirose et al.[102,133] to bond Cu substrates, in which the paste contained a large amount of organics to support the reaction of Ag_2O, and this reduced the bonding temperature to 180 °C. The organics in the pastes of the above two methods have been limited, thus further reducing temperatures. If the paste content incorporates less organics, the bonding temperature could decrease to 150 °C or

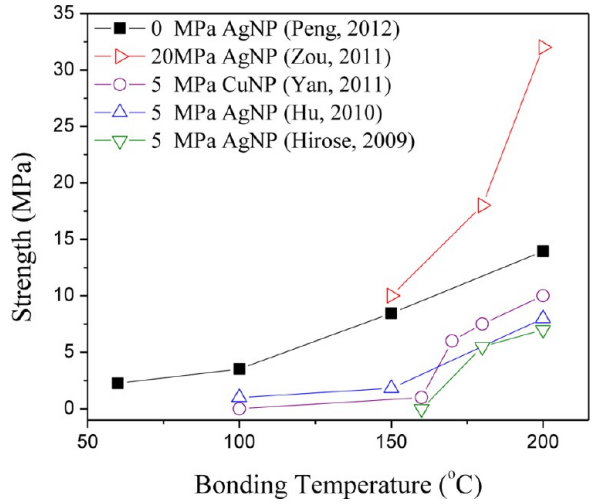

Figure 5. Strength of joints bonded at different temperatures (data points adapted from refs 50, 88, 102, 106, 129).

even lower with further tuning of the particle size distributions (will be discussed separately in a later section), as demonstrated by Zou et al.[129] and Hu et al.[88] Although increasing temperatures clearly enhance diffusional bonding, coarsening and coalescence of nanostructures also occur, which ultimately deteriorate the microstructure and disrupt the properties that are enhanced at the nanoscale.

3.3.2. Time. Time is another factor controlling the sintering process as mentioned in Section 3.1 and will affect the joint strength eventually. At the same sintering temperature, longer sintering time could allow the organics or solvents to decompose and more NPs interconnect with their near neighbors to increase the density of sintered nanomaterials and improve the joint strength. Figure 6 summarizes the joint strength recorded at various sintering times from a few seconds to 60 min. A nearly linear relation between strength and sintering time at 250 °C was reported by Hirose et al.[102] using in situ formed Ag NPs, as open squares plotted in Figure 6. At the same time, the coarsening of NPs must be considered when

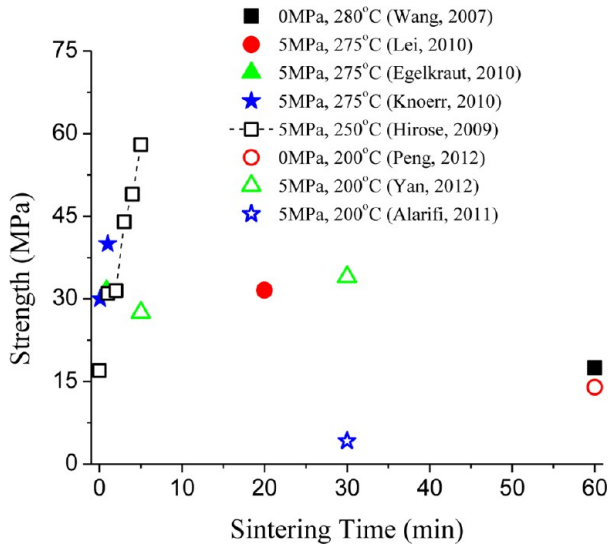

Figure 6. Strength of joints bonded with Ag nanomaterials at different sintering times (data points adapted from refs 45, 93, 97, 98, 100, 102, 106, 134).

DOI: 10.1021/acsami.5b02134
ACS Appl. Mater. Interfaces 2015, 7, 12597−12618

the sintering time increases because grain growth instead of densification of sintered nanomaterials naturally leads to lower joint strength.[55] Herein, higher sintering temperature might be better to further improve the strength since it could help densify the sintered nanomaterials due to the grain boundary and lattice diffusion of interconnected nanomaterials, which are also referred to as densification mechanisms at higher temperature in the literature.[55,134] For example, using an external pressure of 5 MPa at 200 °C, the joint strength increased from 28 to ~35 MPa when sintering time was increased from 5 to 30 min.[93] However, when the temperature increased to 275 °C, 40 MPa was recorded after only 1 min of sintering at the same pressure.[98]

3.3.3. Pressure. When the particle size decreases to the nanoscale, the sintering pressure between two contacting spherical particles will increase as suggested in Section 2.2. The application of external pressure during a sintering process could enhance this sintering pressure and also help densify the sintered nanomaterials and improve the joint strength. Figure 7

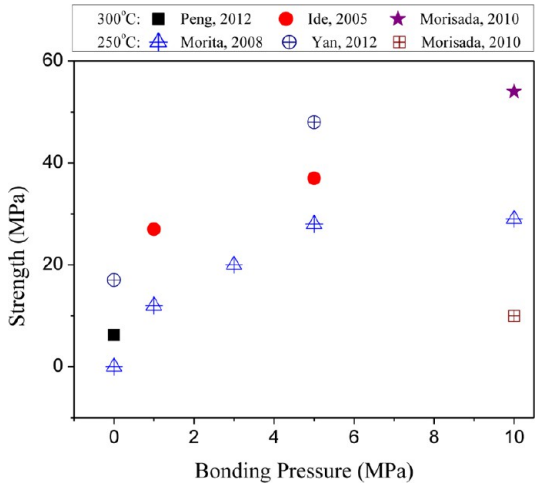

Figure 7. Strength of joints bonded at different external pressures (data points adapted from refs 77, 82, 87, 93, 95).

illustrates the influence of bonding pressure on the joint strength. From the work of Morita et al. and Yan et al.,[93,95] the strength exhibited a significant increase when the bonding pressure increased from 0 to 5 MPa at 250 and 300 °C. However, increases in bonding pressure to 10 MPa provided limited improvement in the strength.[95] This threshold bonding pressure of 5 MPa has been reported when the sintering temperature is 275 °C by Lei et al. as well.[55,97] It has been found that this threshold pressure is also dependent on particle size.[97] However, a direct correlation between particle size and threshold pressure is difficult to establish by theoretical modeling since a wide distribution in particle size and irregular particle geometries in experimental studies complicate this issue. Although the bonding pressure has been dramatically decreased using Ag NPs instead of Ag microflakes, the ideal pressureless bonding has been difficult to achieve in practical applications. By tuning the Ag NP surface conditions and organic content in the pastes, pressureless bonding has been demonstrated at low temperatures, which is very helpful for microelectronic packaging[82,93,106,135,136]. Recently, pressureless bonding has also been achieved with Cu NPs by addition of Cu–Ni or Ni–Sn alloy NPs.[51,112] However, it is still a challenge to decrease the porosity of sintered nanomaterials and increase the coverage (as mentioned in Section 3.1) on the substrates to further improve strength and conductivity when no bonding pressure is applied.

3.3.4. Nanoparticle Size and Shape. While the factors discussed above relate to the bonding process, the nanomaterials themselves also play an important role in nanosintering and bonding applications. Since the NP size and shape are two main parameters to influence the joint strength, these issues will be the focus in the following review section.

In Figure 8, the particle size effect on the joint strength is illustrated with the trend that smaller Ag NPs can produce

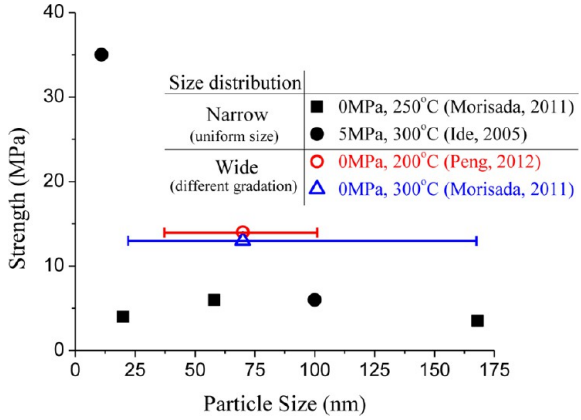

Figure 8. Particle size effect on the strength of sintered nanomaterial joins. Closed symbols indicate that the sizes are uniform in the pastes; open symbols represent average sizes of NPs in the pastes with different gradations, and the size distribution is represented as a line covering a range (data points adapted from refs 87, 101, 106).

higher joint strength because of higher sintering pressure and lower sintering temperature in general. The different packing density of Ag NPs with different sizes is another item that should be considered during nanosintering. Obviously, NPs with a broad size distribution could gain more dense packing and improve the joint strength as demonstrated by our study[106] and Morisada et al.[101] at 200 and 300 °C, respectively. In Morisada's study,[101] three kinds of Ag NPs with mean sizes of 20, 58, and 168 nm were mixed in different fractions: the joint using the trimodal mixture of Ag NPs achieved pressureless bonding with good strength. Thus, size distribution of NPs in the paste could be adjustable to improve the performance of sintered nanomaterials for low-temperature and pressureless bonding applications.

At present, pastes described in published papers have mostly involved NPs; only few have investigated different shaped nanomaterials. In a recent paper, Ag NPs have been partially replaced by NWs.[106] It was found that incorporating a 10% (vol) fraction of NWs could increase the fracture toughness dramatically as indicated in Figure 9a, although the maximum failure forces in the joints were similar. Those NWs in the sintered nanomaterials could act as a second reinforcement phase under loading. The reinforcement mechanism was attributed to necking, breakage, and pullout of NWs, which occurs on loading,[106] according to the observation of areas close to cracks on the fracture surface, as indicated by the behavior of NWs on the fracture surface in Figure 9b. Moreover, binary pastes with NWs and NPs have shown a better joint strength than pure NP paste.[106] However, pure Ag NW pastes can only have competitive performance when the

DOI: 10.1021/acsami.5b02134
ACS Appl. Mater. Interfaces 2015, 7, 12597–12618

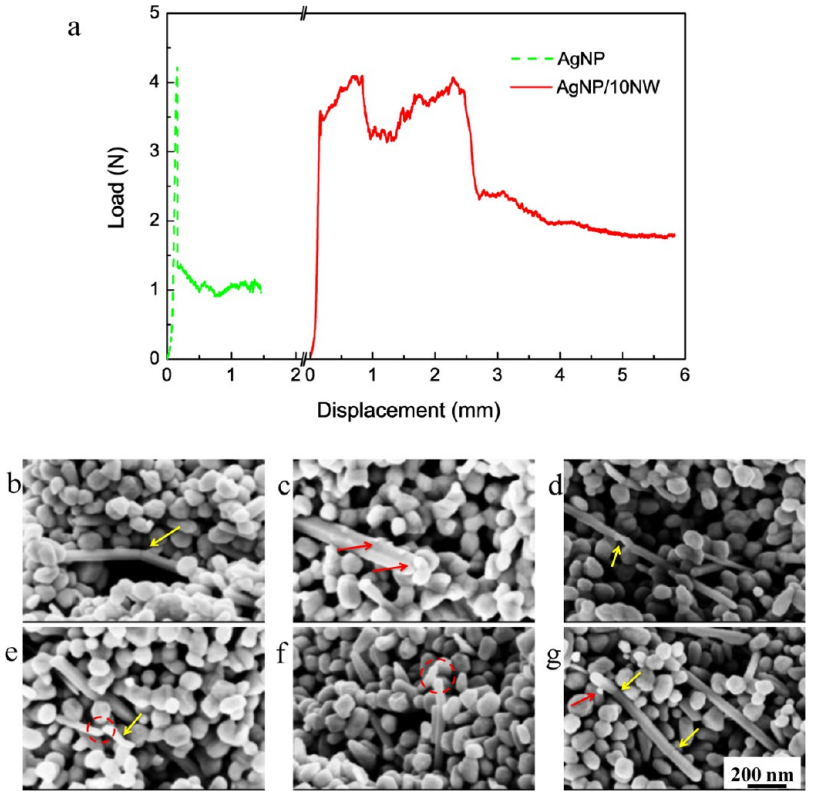

Figure 9. (a) Typical load–displacement curves of bonded joints with AgNP/10NW and Ag NP pastes. SEM images of silver NWs in joints after testing with the enforcement behaviors of (b) NW bent under stress; (c) NW pullout; (d) plastic deformation of NW; (e) NWs broken under stress. Not individually, the combined actions of Ag NWs are illustrated: (f) bent NW was broken into two wires under stress; and (g) NW was bent and pulled out (b–g scale bar is 200 nm). Reprinted with permission from ref 106. Copyright 2012 Springer.

bonding temperature is less than 150 °C; see Figure 10. This might be due to the shape effects of NWs or nanobars, since

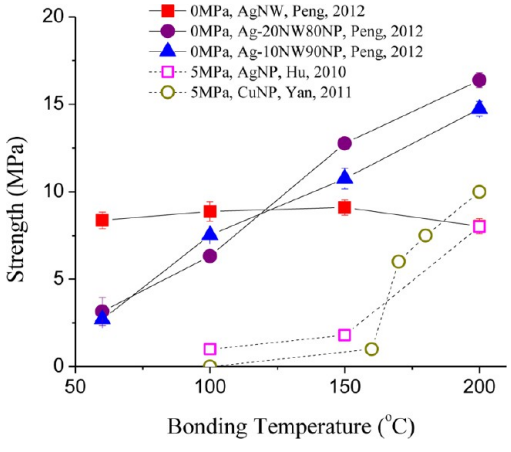

Figure 10. Strength of joints bonded using different pastes at low temperatures (data adapted from refs 50, 82, 88, 106).

they cannot gain a dense packing during nanosintering, which makes the porosity of sintered nanomaterials relatively high when the sintering temperature is above 150 °C. Near room temperature, joints made using NW pastes exhibited 8 MPa strength;[82] however, the detailed reasons have not been reported at present. Therefore, developing different shaped nanomaterials for such nanopastes could provide more insight to understand the nanosintering and resulting mechanical properties under loading.

3.3.5. Presence of Organics in the Paste. Organic content in the pastes, including binder/dispersant and passive layer on NP surface, are the impediments for sintering of Ag NPs. In general, when the organic content is reduced, the sintering temperature can be reduced. Presently, various solvents, such as ethanol and ethylene glycol,[137] methanol,[138] toluene,[139,140] and isopropanol,[141] have been used to remove the dispersant and reduce the required sintering temperature close to room temperature. Utilization of weakly binding organics[131] or easily decomposable organics[128,130,142] on the NP surface could also attain this aim.

Instead of removing the organics, another approach is to utilize them to benefit sintering through paste materials engineering. For example, one could use reactive organics in the paste during sintering, which could react with the used solvent or gas; meanwhile, the reaction heat would further promote the sintering. Also, metal oxide could also be adopted as a precursor that would react with the binder in the paste and in situ transform to metal NPs for joining. This has been demonstrated as an effective method for bonding Cu to Cu with Ag_2O NPs and EG or PEG by Hirose et al.[102,133] Recently, we also found that CuO and PVP might be another couple for the same purpose of electronic packaging.[143]

Through introducing photocatalytic NPs (usually semiconductors, for example, TiO_2) into Ag NP paste, photodecomposition of PVP organic layers on the surface of Ag NPs under UV irradiation to facilitate the sintering at room temperature has been demonstrated as a new route.[144] Although this method is unsuitable for electronic packaging application because the light is difficult to penetrate through the

DOI: 10.1021/acsami.5b02134
ACS Appl. Mater. Interfaces 2015, 7, 12597–12618

entire filler material layer, and the use of semiconductive NPs could reduce the electrical conductivity of joint, it is believed that this photonic decomposition method would be an alternative to sinter nanomaterials on substrates for inkjet application.

4. ELECTRICAL AND OPTICAL PROPERTIES OF SINTERED NANOMATERIAL

4.1. Electrical Conductivity of Sintered Nanomaterial Joints. The excellent electrical performance of silver makes it a desirable candidate material for electronic applications. Most of the electrical conductivity measurements are focused on the sintered nanomaterial thin films for transparent electrode and inkjet printing electronic applications. Few results exist on sintered nanomaterial joints, which have been discussed in Section 3.3. Here, only the performance of such joints will be reviewed rather than thin films. Since the sintered nanomaterials are relatively thin between two substrates, the electrical conductivity of such materials is difficult to measure. Generally, the electrical conductivity of sintered silver nanomaterial joints relates to the porosity of the joint associating with the sintering parameters[145] and its chemical composition[146] as well.

The four-probe method has been used to test the resistivity of bonded joints using Cu NP and Ag NW pastes. For Ag NPs and Ag NWs, the sintered nanomaterial joints acquire low resistivity, which is only one order larger than the bulk Ag at various sintering temperatures as shown in Figure 11a.

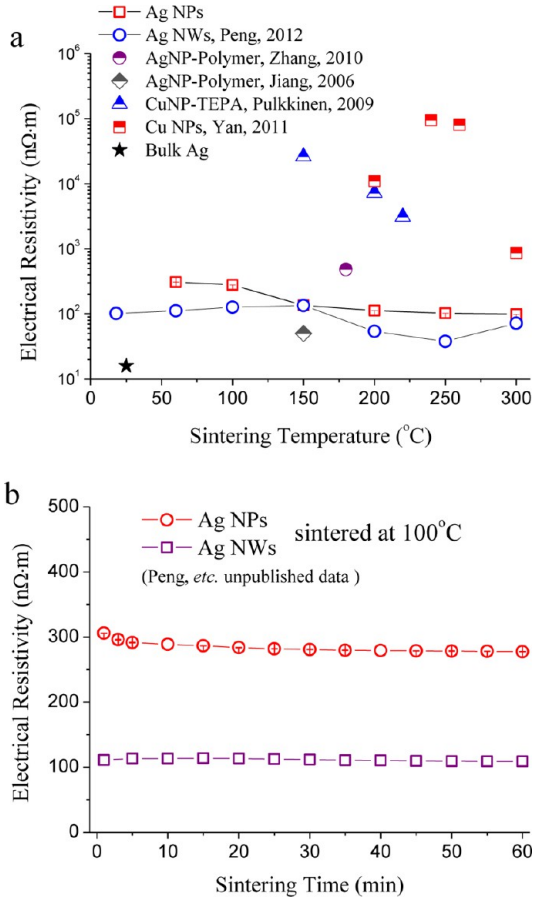

Figure 11. Electrical resistivity of nanomaterials at different (a) sintering temperatures and (b) sintering times (data points adapted from refs 50, 82, 147−149).

Combinations of Ag/Cu NPs have also been introduced into polymers to improve their conductivity. These sintered nanomaterial−polymer composites reached ultralow resistivity.[147−149] At low temperature, the conductivity of sintered nanomaterials will not increase significantly with prolonged sintering time, as demonstrated by the sintering results at 100 °C for 1 h in Figure 11b. When the temperature increased, under prolonged sintering times, the resistivity dramatically decreased, as Jiang et al. reported in Ag NP−polymer composites.[149] This might be due to the increased density and more intense sintering by elevated temperatures as discussed in relation to the mechanical properties in Sections 3.3.1, 3.3.2. It is worth noting that different shapes of Ag nanomaterials might have different electron-transport modes, suggesting that the conductivity of such sintered nanomaterials from different shapes will differ, as in the case of the Ag NP and NW shown in Figure 11b. At this moment, the mechanism is still unclear.

4.2. Effective Contact Area and Electrochemical Migration. For electrodes or films, the sheet resistance is less influenced by the interface condition between nanomaterial layer and substrates. However, the resistivity of sintered nanomaterial joints should contain the influence of this interface (between sintered nanomaterials and substrates) besides that of the porosity of the nanomaterials themselves. As discussed previously, the coverage of nanomaterials on substrates will affect the mechanical properties of the joints, although the uniformity and degree of coverage is difficult to control. This also influences the transport pathways of electrons from a bulk component to another via the sintered nanomaterials. For example, low coverage will reduce the effective contact areas between nanomaterials and substrates, as illustrated in Figure 3c. However, the calculated resistivity is based on the coated area at the macroscale, which is larger than the effective contact areas. Thus, the effective contact areas for electron pathways are a vital factor to evaluate the conductivity of sintered nanomaterial joints.

The microstructure change and the reliability of joints caused by electrochemical migration of nanomaterials when applying electrical potential during service also needs to be studied for power electronics at different temperatures.[150−152] Applying long-term bias voltage, the nanomaterials could fracture because of the electrochemical migration of atoms under electrical potential. In one study by Heersche et al., a thin Au electrode was observed in situ under TEM after applying bias.[153] The results suggested that voids would form and that necks between particles would narrow and break during a short time; see Figure 12. Silver has a larger electrochemical migration rate than that of gold and copper in general. Therefore, the failure of silver-sintered nanomaterial joints caused by electrochemical migration effects will need to be further studied since these conductive joints will undergo a long-term current loading in practical applications.

Lu et al. have conducted the electrochemical migration test of sintered Ag nanomaterials at high temperatures on aluminum nitride (AlN)[151] and alumina (Al_2O_3)[152] substrates in dry air condition. Figure 13a illustrates the spaced Ag NP electrodes on AlN substrate. The testing temperature was 500 °C with a direct-current (DC) bias applied on electrodes; see Figure 13b,c. It was found that the Ag dendrites were easier to form on Al_2O_3 than on AlN substrate at different voltages, electrode spacing, and temperatures to short the electrode as the leakage current is larger than 1 mA.[151] This may be due to

DOI: 10.1021/acsami.5b02134
ACS Appl. Mater. Interfaces 2015, 7, 12597−12618

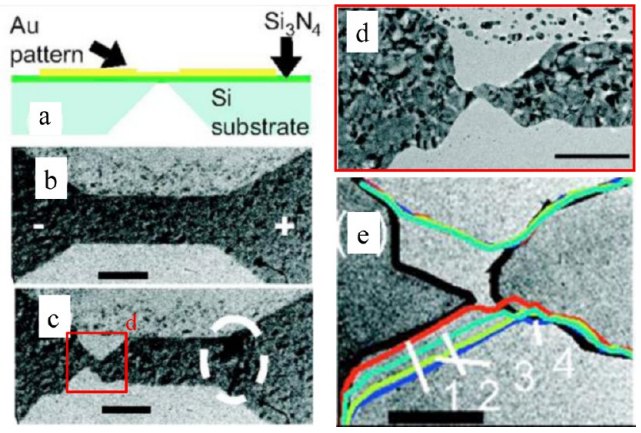

Figure 12. (a) Cross section of experiment setup for in situ TEM observation. (b) Initial (polycrystalline) 12 nm thick Au wire by ramping a bias voltage before breaking. (c) Necking (□) and hillocks at the anode side (○) after applying voltage. (d) High-resolution overview of necking area. (e) Formation of gap by electrochemical migration; the line numbers 2−4 correspond to the outer surface of the Au wire recorded at 100, 200, and 300 ms earlier, respectively. The wire finally broke along the grain boundary with a final gap size of 6 nm. Scale bars: 200 nm (b−d) and 20 nm (e). Reprinted with permission from ref 153. Copyright 2007 AIP Publishing LCC.

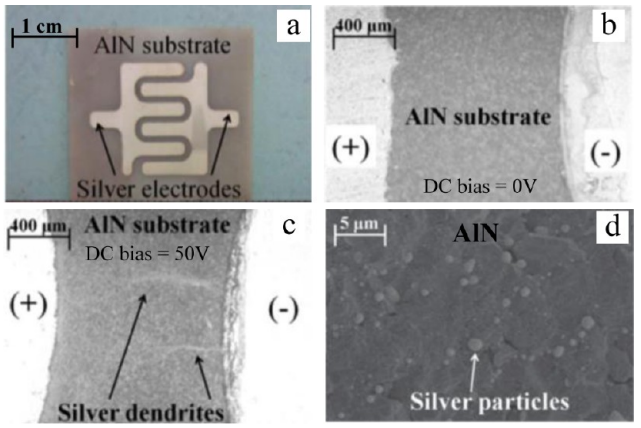

Figure 13. Electrochemical migration test of sintered Ag nanomaterials at high temperature. (a) Sintered Ag nanomaterial electrodes with 1 mm spacing on AlN substrate for testing. Optical images of sintered Ag nanomaterial electrodes after 119 min at 500 °C (b) without bias and (c) with DC bias of 50 V. (d) SEM image of formed Ag NPs on AlN substrate due to migration. Reprinted with permission from ref 151. Copyright 2014 IEEE.

the high diffusivity and high ionic conductivity of the boundaries of Al_2O_3 particles for distributing Ag particles compared with AlN substrate. Figure 13d shows the Ag particles presented on the AlN surface due to migration. Large amounts of these Ag particles would form dendrites first and further cause the bridging of electrodes. Ag would dissolve into Ag^+ at anode, while H^+ from H_2O discharges to maintain the electrical balance. The Ag^+ could migrate on the surface of substrates and combine with OH^- to form AgOH, which could decompose into Ag_2O and then Ag at high temperatures.[152] Oxygen in the air was speculated to play important roles as H_2O did to assist the Ag migration under electrical potential in this process. However, the exact underlying mechanisms still remain unclear and need to be further elucidated both experimentally and theoretically.

4.3. Optical Properties. By changing the shapes and sizes of Ag nanomaterials, many applications have been reported based on their plasmonic properties, such as optical sensors, surface-enhanced Raman scattering probes, or light filters.[10,154−156] For example, the absorption band of Ag NP thin films has been tuned by changing the nanosintering of Ag NPs under thermal and laser irradiation.[10,157,158] At present, surface-enhanced Raman spectroscopy (SERS) is an attractive topic for using silver nanomaterials with different original shapes, such as plate,[154] cube,[159] rod,[160] and wire.[161] To construct more complicated shapes, bottom-up assembly or nanojoining of Ag building blocks is more efficient. Nanoparticles that are assembled with weak interaction, that is, van der Waals force, are disassembled easily, whereas those NPs assembled with strong metallurgical bonds will produce stable shaped probes for Raman signal or other optical applications. Further, according to simulated results, joined NPs may contain an increased number of hot-spot areas compared with single or adjacent NP pairs;[42,162] see Figure 14a. A few reports have

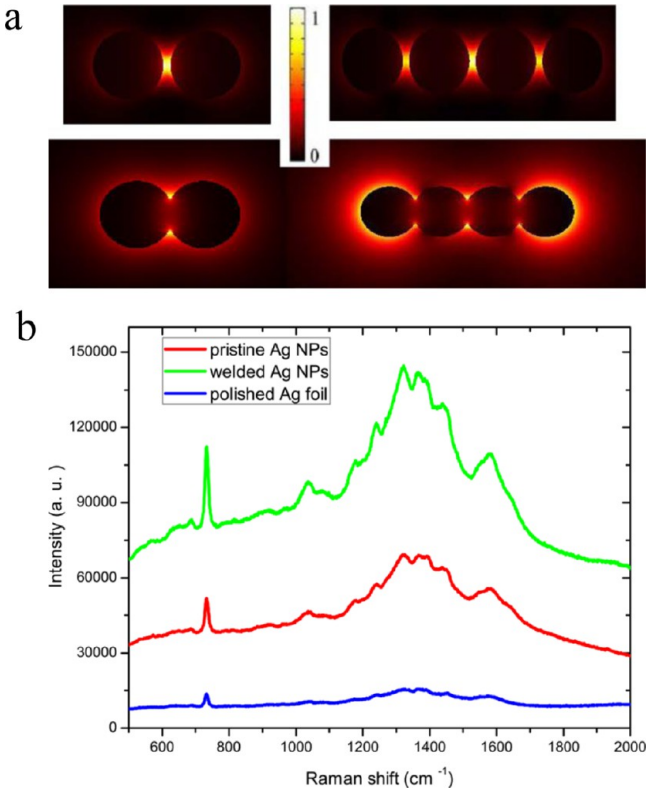

Figure 14. (a) The cross-sectional views of normalized electric field distributed at the surface of the nanostructures in air. (upper) Adjacent two and four Ag spheres with a diameter of 50 nm and a central gap of 5 nm. (lower) Welded two and four Ag spheres at the same diameter and an overlapped central distance of 5 nm (i.e., the central gap of −5 nm). (b) Demonstration of joined Ag NPs for SERS with adenine molecule. Reprinted with permission from ref 42. Copyright 2012 Laser Institute of America.

involved the SERS applications of joined Ag NPs;[42,163] see Figure 14b. However, the joined Ag nanoplates or other highly symmetrical Ag nanomaterials are expected to exhibit different optical properties. Therefore, under a nanoscale electromagnetic field, a deeper understanding of the structure effects on the optical properties of Ag nanomaterials, having different

DOI: 10.1021/acsami.5b02134
ACS Appl. Mater. Interfaces 2015, 7, 12597−12618

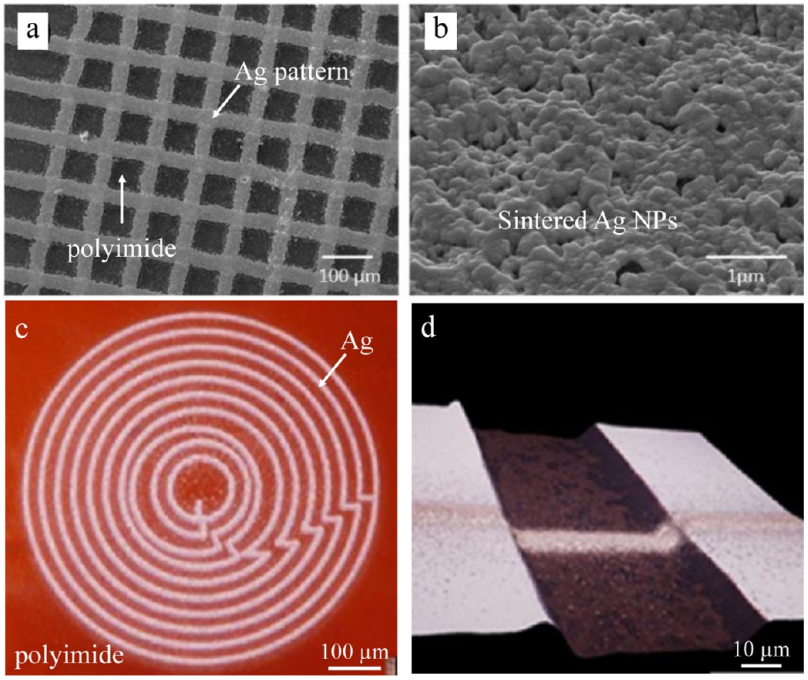

Figure 15. SEM images of (a) aerosol jet-printed and (b) thermally sintered Ag lines. (c) Aerosol jet-printed spiral Ag pattern on polyimide substrate. (d) Topographical image of printed Ag line over a 10 μm deep trench on Si. Reprinted with permission from ref 168. Copyright 2013 ACS Publications.

original shapes and different crystallographic facets, will open doors for new applications.

5. APPLICATIONS IN PRINTABLE ELECRONICS

In addition to the packaging of power electronics, low-temperature joining of Ag NPs could benefit the fabrication of printable electronics, especially on flexible substrates (e.g., poly(ethylene terephthalate), polyimide, etc.), which has become a new application area for Ag NP paste. Direct writing methods have been developed using selective laser sintering of Ag NPs for conductive tracks.[164] Typically, a layer of Ag NP paste is spin-coated on glass or polymer substrates and followed by the selective laser sintering process with a focused laser beam (e.g., Nd:YAG, 532 nm) to rapidly scan and join the Ag NPs converting into various patterns.[165] The residual NPs, which remain unsintered, can be removed by organic solvents. Unlike the conventional lithography, this rapid process can be used for large-area electronic fabrication without using a photomask. Because of the use of focused laser beam, most laser sintering processes of Ag nanomateirals involve high temperature locally, which might reach or exceed the melting temperature of Ag NPs[10] and cause the damage of used substrates, particularly plastic substrates. Therefore, the laser power and scan speed should be carefully controlled. Besides, the technical barrier and increasing cost due to the removal of residual Ag NPs should be considered.

Instead of the coating-selective sintering-removing processes, one could print the expected patterns on the substrates using Ag NP paste. At present, the printing methods mainly include inkjet,[166,167] aerosol jet,[168] and screen[169] printings, which are rapid and also easy to control at microscales. By tuning the NP size, binder, dispersant, and solvent in the paste (or ink, sol), Ag NPs can be sintered at low temperatures as discussed in Section 3. Such printed NP patterns on the substrates can be heated at 75 to 200 °C to sinter NPs.[165−168,170] Figure 15a shows the aerosol jet-printed Ag NP patterns on polyimide. After they were sintered, the Ag NPs were joined together with a porous structure (see Figure 15b). These aerosol or ink jet printing methods can reach the resolution of a few microns depending on the used nozzles and moving stages. For example, in aerosol jet printing, Ag NPs (aerosol streams) are carried by the carrier gas, and aerosol beam can be focused aerodynamically by sheath gas inside the print head. Therein, the geometry of printed Ag lines could be controlled by the flow rates of gases in the printing head. Figure 15c displays a spiral Ag pattern using this technique indicating it has the capability of printing complex and high-resolution patterns. It is also worth mentioning that the defects of printed lines, in particular, cracking and peeling after drying and sintering, must be considered when evaluating the quality of printed lines. Fortunately, unlike in Ag microflake paste, this problem is rarely reported in Ag NP paste. It is suspected that the Ag NP patterns containing smaller particles could withstand bigger deformation than microparticles. Also, the binders in the paste more easily bind the NPs compared with microparticles. Therefore, printing complex structures or even three-dimensional patterns would be possible using this method, as indicated by the Ag line crossing a 10 μm deep trench without cracking and peeling shown in Figure 15d. Moreover, the cracking and peeling defects of printed Ag NP lines could be overcome by systemically controlling the drying and sintering parameters, the interfacial bonding between Ag NPs and substrates, and the composition of the pastes.[171]

Ag nanomaterials have also been introduced into polymer matrix to fabricate electrically conductive adhesives. It is also a low-temperature process, and such conductive adhesives can be used as printing or packaging materials for electronics as well.[172] Since the conductivity normally contributes by the contact of Ag nanomaterials in adhesives, which is also quite complex due to the presence of thick polymer at Ag

DOI: 10.1021/acsami.5b02134
ACS Appl. Mater. Interfaces 2015, 7, 12597−12618

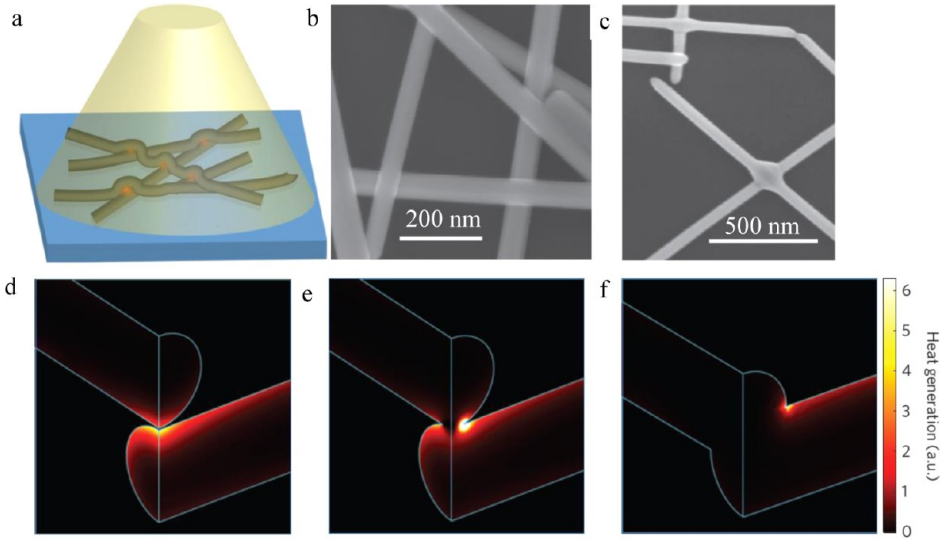

Figure 16. (a) Optical nanowelding setup and scanning electron microscope (SEM) images (b) before and (c) after optical welding of Ag NWs with a tungsten halogen lamp. (d–f) Finite element method simulations of optical heat generation at Ag NW junctions during the nanowelding process. Reprinted with permission from ref 40. Copyright 2012 Nature Publishing Group.

nanomaterial interface, it is beyond the scope of this review and will not be discussed in detail. Usually, spherical NPs in the matrix (for example, polydimethylsiloxane) might have less contact opportunity to form a conductive network than other shaped nanomaterials given the similar amount of Ag addition. One-dimensional structures, such as Ag NWs and belts, may significantly increase the conductivity.[173]

6. OTHER NANOJOINING PROCESSES AND APPLICATIONS

Thermal sintering for microjoining and macrojoining requires high temperatures to promote atomic interdiffusion to form a metallic bond. Further, thermal sintering is not an area-specific method for joining nanoscopic building blocks. During the heating process, it is difficult to control the sintering level. However, the shape and size of nanomaterials are two key factors that are vital for fully exploiting their properties. Because of the nanoscale effect, the nanomaterial will be more active because of the lower melting points and larger portions of atoms on the surface than bulk materials. These would help to maintain the shape of nanomaterials for using their unique optical or electronic properties. Thus, more precisely controllable low-temperature or even room-temperature joining methods are required.

In this section, some recently developed low-temperature joining methods are discussed, where most of them are active at room temperature and can maintain the original shapes of the nanomaterials.

6.1. Optical Welding: Localized Plasmonic Heating. Light will induce heating of materials due to absorption of radiation; for example, pulsed lasers with high energy density may induce rapid heating and melting in a short time for sintering.[16,174−176] This energy source requires improved control for welding of nanomaterials. Recently, the use of a tungsten[40,177] or xenon[178,179] lamp was demonstrated in fabricating large area conductive electrodes or thin films on paper and plastic substrates. Camera flash has also been used as light source to sinter Ag NP tracks[180,181] or reduce the sheet resistance of Ag NW electrodes for foldable paper electronic application.[182] Garnett et al.[40] explained this as a self-limited plasmonic welding method to create nanojunctions of Ag NWs, as shown in Figure 16a−c. In this scenario, by using the plasmonic effect of silver, a low density of light will concentrate at the gaps between two adjacent nanoobjects, and these areas are referred to as hot spots. This concentration of light can induce a high temperature locally without heating the surroundings as suggested in the simulated results in Figure 16d. Thus, local melting can occur and form metallic bonds at the interfaces, keeping the rest of the NWs with their original shape. However, it is not an area-specific method, and joint quality will depend on the lighting time, light intensity, interface geometries, and the separation distances between nanomaterials because of the limited size of the hot spots. Nevertheless, selective plasmonic welding might be interesting for nanodevice fabrication in the future.

6.2. Ultrafast Laser Joining: Controllable Spatial Heating. Ultrafast pulsed laser, in particular, femtosecond (fs) laser, has become a commonly applied source for nanojoining with controllable spatial heating, which has drawn much attention recently.[163,183−186] Because of the ultrafast nature of the fs laser, during the first few pulses, the thermal effect is limited when laser interacts with nanomaterials. An added benefit is the localized surface plasmon energy delivered to the discontinuous joint locations on the nanomaterial surface and thus helps promote joining with lower energy input. Liu et al.[187] have reported that fs laser-induced plasmon excitation could be locally controlled in one single Ag NW, in which local heat will be a useful source for controllable selective joining of individual Ag NWs. The direction of polarization of laser was found to be an important factor affecting the plasmon excitation when irradiating Ag NWs.[188] Ag filler materials were studied for fs laser joining of Pt−Ag alloy NPs in an aqueous solution; it was found that the lattices between Ag and Pt−Ag showed a good matching along (111) planes, which might be due to a melting and solidification during joining process.[189] When PVP-coated Ag NPs were irradiated by fs laser in solution, the radiation could graphitize the PVP layer and change the surface condition of Ag NPs to increase the surface diffusion for joining of Ag NPs; see Figure 17a,b. The joined Ag

DOI: 10.1021/acsami.5b02134
ACS Appl. Mater. Interfaces 2015, 7, 12597−12618

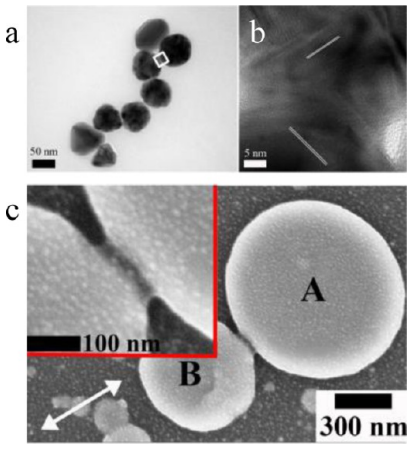

Figure 17. (a) TEM and (b) HRTEM images of Ag NPs irradiated by fs laser pulses (35 fs) for 20 min at 0.2 mJ/cm^2 in water. Reprinted with permission from ref 163. Copyright 2015 IOP Publishing. (c) Ablated Ag NPs irradiated with laser pulses (35 fs) at 0.9 mJ/cm^2 for 50 s on Si substrate. Reprinted with permission from ref 190. Copyright 2012 AIP Publishing LCC.

NPs have shown a great signal enhancement for SERS application. These processes are with long irritation time (>1 min) or high laser fluence (>10 mJ/cm^2), at which conditions the heat could accumulate to induce melting (or partial melting) of nanomaterials. If the irritation time or pulse repletion rate and laser fluence is reduced, one can expect that the heat effect could be weakened during laser-material interaction. Figure 17c gives the ablated Ag NPs irradiated for 50 s at 0.9 mJ/cm^2.[190] Along the laser polarization direction (arrow indicated), the gap has been filled with materials, while no apparent damage was found near the joining area (inset of Figure 17c).

6.3. Pressure Joining: Plastic Deformation. Plastic deformation has been used in joining of bulk materials during ultrasonic wire bonding,[191] roll bonding,[192] forge welding,[193] and friction stir welding.[194,195] However, these methods involve friction or severe deformation at the interfaces and generate extensive heat, to nearly the melting point of the material, which is difficult to control in the case of nanomaterials. Because of the small interface of two nanomaterials, a small external force will produce large pressure for plastic deformation. If friction is absent, nanomaterials may join under such high pressure at room temperature. A simple approach has been demonstrated using this idea as illustrated in Figure 18a,b. By applying pressure of 25 MPa on the Ag NW thin film and holding only 5 s, these NWs were cross-linked and formed junctions, showing an ultralow sheet resistivity.[196] In this study, the microstructure of local interfaces was not shown, and the interconnection mode (metallic or mechanical) was unclear. Further, this is not an interconnection area specific approach since the external pressure is applied on a large area. Thus, selective joining using pressure-induced plastic deformation will be another interesting topic needing to be studied. Recently, nanoindentation has been used as a useful tool to select the joining area and perform precise joining of Ag NW with large plastic deformation as shown in Figure 18c,d.

6.4. Ion-Activated Joining: Removal of Passive Layers. Usually, a thin organic layer is coated on surfaces of nanomaterials to reduce oxidation because of the high surface energy when material size decreases to the nanoscale. This passive layer at the interface will restrain atomic diffusion. It is difficult to remove since the organic compounds are stable at room temperature until they are heated to their decomposition temperature or dissolved in certain solvents. Because of the high diffusion rate at the nanoscale, interdiffusion occurs automatically when two clean interfaces are brought into close proximity. This will promote room-temperature joining when particle arrays are treated with different solvents to remove passive layers, as demonstrated in Figure 19. Presently, the ion solution used in the reported methods involves two main categories, namely, cationic polymers and electrolyte solutions. For example, poly(diallyldimethylammonium chloride) is one of the polymers used in Magdassi et al.'s study.[197] Solutions of NaCl, $MgCl_2$, and $CaCl_2$ were adopted to trigger the sintering of Ag NPs as well.[198−201] Also, the reduction of Ag NW-to-NW junction resistance has also been realized by immersing Ag NW

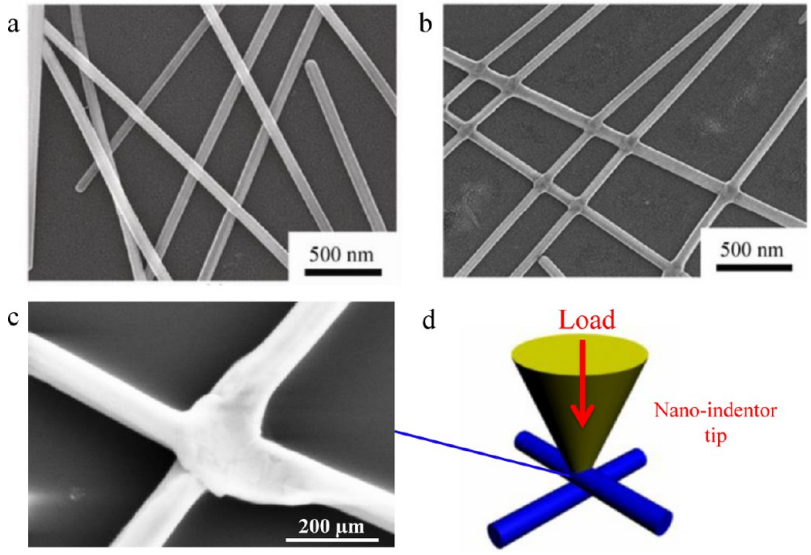

Figure 18. Ag NW film: before (a) and after (b) applying 25 MPa pressure for 5 s. Reprinted with permission from ref 196. Copyright 2011 Springer. (c) Single Ag NW junction formed by plastic deformation using (d) nanoindentation.

DOI: 10.1021/acsami.5b02134
ACS Appl. Mater. Interfaces 2015, 7, 12597−12618

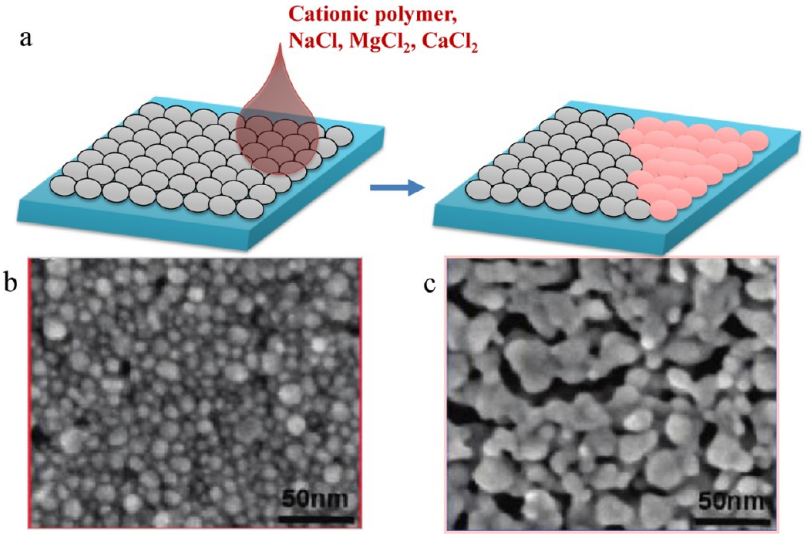

Figure 19. (a) Schematic illustration of chemically activated joining using cationic polymer or electrolyte solution. The microstructure of Ag NPs before (b) and after (c) applying cationic polymer. Reprinted with permission from ref 197. Copyright 2010 ACS Publications.

film in a boiling $HAuCl_4$ aqueous solution[202] and through an electroless deposition process with Ag^+ and reducing agent to enhance the deposition of Ag right at the junctions.[203] However, the mechanism for removal of organics in these solvents is unclear at this moment. In general, all these usable solvents contain Cl^{1-} to help desorption of protective organics on the surfaces. However, Cl^{1-} or other ions will also leave residue on the nanomaterial surfaces significantly influencing their chemical properties. Changes in the shape of Ag NPs may also occur after immersing them into solutions with high concentrations of ions. Further, this approach is not area selective since the entire surfaces would be exposed after removing the organics. However, it will be a potentially efficient and programmable method to fabricate conductive films or electrodes due to the complete removal of organics.

6.5. Self-Joining: Self-Oriented Attachment. When the interface is free of barrier organic layers, interdiffusion will form metallic bonds as discussed in the chemically activated joining method. However, in this approach, the surface is only partially activated for joining, suggesting it is an area-selective joining method. Meanwhile, self-orientated attachment of nanomaterials as a key mechanism[26,35] will largely reduce the interfacial energy and defects,[204] allowing the joined materials to contain fewer defects, which is important for nanocircuits. With the help of in situ TEM, two Au NWs were brought into contact in head-to-head and side-to-side modes using a nanomanipulator, and the joining process was observed, as shown in Figure 20a,b.[26] They formed a metallic joint after ~2 and 4.5 min, respectively. Recently, this joining process has also been reported on Ag NWs.[35] V-shaped joints can be formed with certain angles by a simple washing process with purified water. The ends of Ag NWs will be selectively activated while keeping the rest of each NW protected with an organic coating that is slightly thicker on the sidewalls of the NWs. Because of the twinning structures in these Ag NWs, the self-orientated attachment will produce V-shaped (or zigzag) single crystalline prisms after joining, see Figure 20c. Recently, this type of self-oriented joining has also been observed in triangular and hexagonal silver nanodisks with TEM observation and molecular dynamic simulation.[69] This joining approach

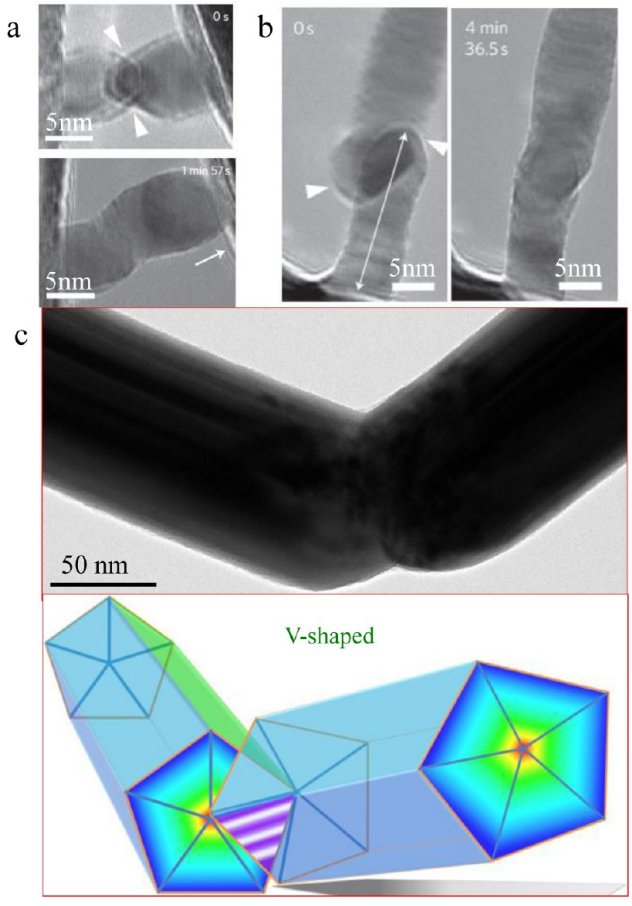

Figure 20. Self-joining of (a, b) Au NW and (c) Ag NW. (a, b) Reprinted with permission from ref 26. Copyright 2010 Nature Publishing Group. (c) Reprinted with permission from ref 35. Copyright 2013 Wiley-VCH.

generating minimal interfacial defects will open areas for many new applications in nanocircuit construction.

6.6. Oriented Assembly: Polymer-Induced Nonpermanent Joining. Self-assembling has become one type of "joining" method to be studied quite widely. However, self-

DOI: 10.1021/acsami.5b02134
ACS Appl. Mater. Interfaces 2015, 7, 12597−12618

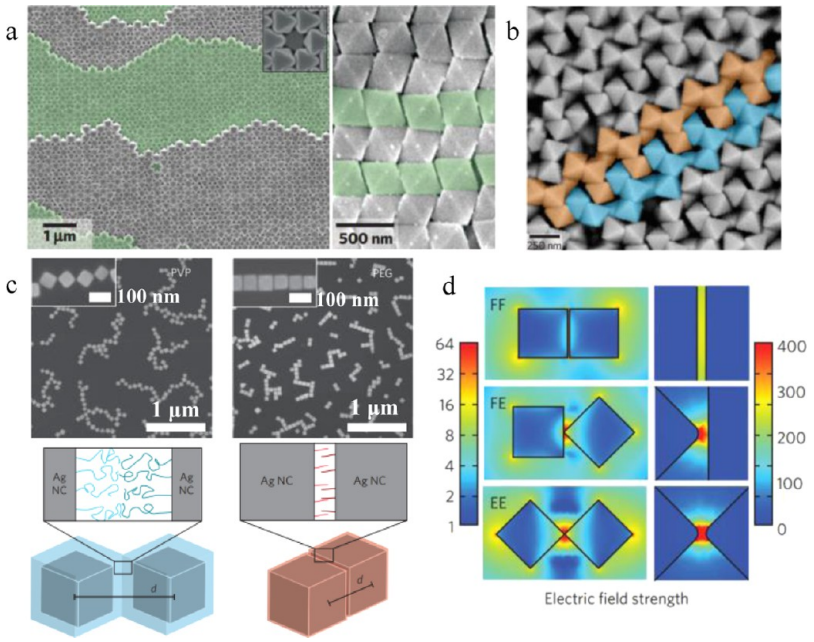

Figure 21. (a) Top-down view (left), with inset showing a vacancy in the lattice, and side view (right) of assembled Ag nanopolyhedrons. (b) Ag nanooctahedra assemble into a lattice consisting of tetramer motifs (color coded) in the presence of excess PVP. Reprinted with permission from ref 206. Copyright 2012 Nature Publishing Group. (c) Edge-to-edge and face-to-face assembly of Ag nanocubes. (d) Electric field strength representation of plasmonic response of different configurations of assembled nanocubes with edge lengths of 80 and 2 nm gap. Reprinted with permission from ref 207. Copyright 2012 Nature Publishing Group.

assembling cannot produce permanent interconnection between two objects because it is based on the interaction of polymers. That is, metallic bonds could not be formed in the case of Ag nanomateirals. To a certain extent, it can be categorized as joining because this method could integrate nanomaterials to form a particular shape or pattern. Henzie et al.[205] have demonstrated that Ag polyhedrons can self-assemble into grooves with different shapes and sizes for reproducible SERS. Also, they can form a macroscale dense packing as shown in Figure 21a and exotic supperlattice as shown in Figure 21b with long-range order, where the gravity and van der Waals attraction played important roles during assembling.[206] By varying the polymers on the surface, such as PVP or PEG with different chain lengths,[207] Ag nanocubes could also assemble together with edge-to-edge or side-to-side manners; see Figure 21c. With certain configurations, the plasmonic effect of assembled structures exhibited large enhancement as the electric field strength indicated in Figure 21d. All these assemblies have facilitated the design of engineered materials for sensing[154] or photocatalysis.[208]

7. CONCLUSIONS AND OUTLOOK

This review has summarized the development of low-temperature joining of silver nanomaterials. For low-temperature bonding applications, various processing factors that would influence the thermal, mechanical, and electrical properties of sintered silver nanomaterial joints have been discussed, such as sintering temperature, sintering time, sintering pressure, and particle size and shape of silver nanomaterials. The porosity of sintered nanomaterials and coverage of substrates have been linked to evaluation of their properties. Furthermore, new applications of sintered silver nanomaterials for printable electronics and in biosensing using their optical properties were also reviewed. Finally, recent developments in room-temperature joining strategies and underlying mechanisms for silver nanomaterials have been highlighted, including plasmonic effect induced heating and welding, pressure induced plastic deformation and joining, chemically activated interfaces for joining, and self-oriented attachment for joining.

Silver NP pastes or ink have already attracted great attention to fabricate conductive joints, films, and electrodes for flexible and printable electronic applications.[182,209] Whether in a completely new or conventional thermal sintering method, low-temperature sintering of silver nanomaterials is still at its infancy stage and demands a more detailed understanding of sintered material properties and possible applications. For example, most mechanical or electrical properties were tested on either individual nanocrystals[210,211] or sintered materials.[212,213] However, the understanding of correlations between these nanoscale properties and the corresponding bulk properties is insufficient. Fundamental research on sintering behavior between different crystallographic facets of silver nanomaterials and dissimilar joining of metallic nanomaterial[214] still needs to be conducted. Those well-accepted concepts at macro- and/or microscale, such as terminologies (welding, sintering, bonding, joining), surface versus bulk diffusion, and solid versus liquid state, will become indistinct or even without identifiable boundaries in some cases at nanoscale. At present, although some new nanosintering approaches have been reported for silver nanomaterials, more systematic studies are needed to unveil the joining mechanism at the nanoscale. It is worth noting that even in joining the bulk materials, the initial stage is also dominated by the joining of nanoscale asperities. Therefore, experimental observation using in situ TEM[214] combined with molecular dynamic simulation[215,216] will provide better understanding of the detailed mass transport in nanosize. Finally, the performance of porous sintered structures and their stability during long-term service is another practical issue to be investigated. The porous sintered

DOI: 10.1021/acsami.5b02134
ACS Appl. Mater. Interfaces 2015, 7, 12597−12618

nanomaterials may open new horizons for applications in biochemistry, such as catalysis and supersensitive sensing.

AUTHOR INFORMATION

Corresponding Authors

*E-mail: nzhou@uwaterloo.ca. (Y.N.Z.)
*E-mail: p5peng@uwaterloo.ca. (P.P.)

Author Contributions

The manuscript was written through contributions of all authors. All authors have given approval to the final version of the manuscript.

Notes

The authors declare no competing financial interest.

ACKNOWLEDGMENTS

Support from the Canadian Research Chairs (CRC) program, strategic research projects of National Sciences and Engineering Research Council (NSERC), National Natural Science Foundation of China (Grant Nos. 51375261 and 51075232), Natural Science Foundation of Beijing (Grant No. 3132020), State Key Laboratory of Automotive Safety and Energy, and Tsinghua University (Grant No. 2013XC-B-02) is gratefully appreciated. P.P. also acknowledges the financial support of the State Scholarship Fund of China (No. 2010640009).

REFERENCES

(1) Zhang, Y.; Dai, H. Formation of Metal Nanowires on Suspended Single-Walled Carbon Nanotubes. *Appl. Phys. Lett.* **2000**, *77* (19), 3015−3017.

(2) Hong, B. H.; Bae, S. C.; Lee, C.-W.; Jeong, S.; Kim, K. S. Ultrathin Single-Crystalline Silver Nanowire Arrays Formed in an Ambient Solution Phase. *Science* **2001**, *294* (5541), 348−351.

(3) Mbindyo, J. K.; Mallouk, T. E.; Mattzela, J. B.; Kratochvilova, I.; Razavi, B.; Jackson, T. N.; Mayer, T. S. Template Synthesis of Metal Nanowires Containing Monolayer Molecular Junctions. *J. Am. Chem. Soc.* **2002**, *124* (15), 4020−4026.

(4) Sauer, G.; Brehm, G.; Schneider, S.; Nielsch, K.; Wehrspohn, R.; Choi, J.; Hofmeister, H.; Gosele, U. Highly Ordered Monocrystalline Silver Nanowire Arrays. *J. Appl. Phys.* **2002**, *91* (5), 3243−3247.

(5) Wiley, B.; Sun, Y.; Mayers, B.; Xia, Y. Shape-Controlled Synthesis of Metal Nanostructures: The Case of Silver. *Chem.—Eur. J.* **2005**, *11* (2), 454−463.

(6) He, X.; Zhao, X.; Li, Y.; Sui, X. Shape-Controlled Synthesis for Silver: Triangular/Hexagonal Nanoplates, Chain-Like Nanoplate Assemblies, and Nanobelts. *J. Mater. Res.* **2009**, *24* (7), 2201.

(7) Wei, G.; Zhou, H.; Liu, Z.; Song, Y.; Wang, L.; Sun, L.; Li, Z. One-Step Synthesis of Silver Nanoparticles, Nanorods, and Nanowires on the Surface of DNA Network. *J. Phys. Chem. B* **2005**, *109* (18), 8738−8743.

(8) Zhou, Y. *Microjoining and Nanojoining;* Woodhead: England, 2008.

(9) Zhou, Y.; Hu, A. From Microjoining to Nanojoining. *Open Surf. Sci. J.* **2011**, *3*, 32−41.

(10) Peng, P.; Hu, A.; Zhou, Y. Laser Sintering of Silver Nanoparticle Thin Films: Microstructure and Optical Properties. *Appl. Phys. A: Mater. Sci. Process.* **2012**, *108* (3), 685−691.

(11) SeobáLee, S.; HwanáKo, S. Very Long Ag Nanowire Synthesis and Its Application in a Highly Transparent, Conductive and Flexible Metal Electrode Touch Panel. *Nanoscale* **2012**, *4* (20), 6408−6414.

(12) Spechler, J. A.; Arnold, C. B. Direct-Write Pulsed Laser Processed Silver Nanowire Networks for Transparent Conducting Electrodes. *Appl. Phys. A: Mater. Sci. Process.* **2012**, *108* (1), 25−28.

(13) Goldak, J.; Chakravarti, A.; Bibby, M. A New Finite Element Model for Welding Heat Sources. *Metall. Trans. B* **1984**, *15* (2), 299−305.

(14) Peng, Y.; Cullis, T.; Inkson, B. Bottom-up Nanoconstruction by the Welding of Individual Metallic Nanoobjects Using Nanoscale Solder. *Nano Lett.* **2008**, *9* (1), 91−96.

(15) Nishimura, T.; Mitomo, M.; Hirotsuru, H.; Kawahara, M. Fabrication of Silicon Nitride Nano-Ceramics by Spark Plasma Sintering. *J. Mater. Sci. Lett.* **1995**, *14* (15), 1046−1047.

(16) Perelaer, J.; de Gans, B. J.; Schubert, U. S. Ink-Jet Printing and Microwave Sintering of Conductive Silver Tracks. *Adv. Mater.* **2006**, *18* (16), 2101−2104.

(17) Imholt, T.; Dyke, C.; Hasslacher, B.; Perez, J.; Price, D.; Roberts, J.; Scott, J.; Wadhawan, A.; Ye, Z.; Tour, J. Nanotubes in Microwave Fields: Light Emission, Intense Heat, Outgassing, and Reconstruction. *Chem. Mater.* **2003**, *15* (21), 3969−3970.

(18) Siores, E.; Do Rego, D. Microwave Applications in Materials Joining. *J. Mater. Process. Technol.* **1995**, *48* (1), 619−625.

(19) Pantoya, M. L.; Granier, J. J. Combustion Behavior of Highly Energetic Thermites: Nano Versus Micron Composites. *Propellants, Explos., Pyrotech.* **2005**, *30* (1), 53−62.

(20) Zhou, Y.; Gale, W.; North, T. Modelling of Transient Liquid Phase Bonding. *Int. Mater. Rev.* **1995**, *40* (5), 181−196.

(21) Li, Y.; Moon, K. S.; Wong, C. P. Electronics without Lead. *Science* **2005**, *308* (5727), 1419−1420.

(22) Tu, K.; Gusak, A.; Li, M. Physics and Materials Challenges for Lead-Free Solders. *J. Appl. Phys.* **2003**, *93* (3), 1335−1353.

(23) Frear, D.; Vianco, P. Intermetallic Growth and Mechanical Behavior of Low and High Melting Temperature Solder Alloys. *Metall. Mater. Trans. A* **1994**, *25* (7), 1509−1523.

(24) Coughlin, J.; Williams, J.; Crawford, G.; Chawla, N. Interfacial Reactions in Model Niti Shape Memory Alloy Fiber-Reinforced Sn Matrix "Smart" Composites. *Metall. Mater. Trans. A* **2009**, *40* (1), 176−184.

(25) Cui, Q. Z.; Gao, F.; Mukherjee, S.; Gu, Z. Y. Joining and Interconnect Formation of Nanowires and Carbon Nanotubes for Nanoelectronics and Nanosystems. *Small* **2009**, *5* (11), 1246−1257.

(26) Lu, Y.; Huang, J. Y.; Wang, C.; Sun, S. H.; Lou, J. Cold Welding of Ultrathin Gold Nanowires. *Nat. Nanotechnol.* **2010**, *5* (3), 218−224.

(27) Zeng, X. Y.; Zhang, Q. K.; Yu, R. M.; Lu, C. Z. A New Transparent Conductor: Silver Nanowire Film Buried at the Surface of a Transparent Polymer. *Adv. Mater.* **2010**, *22* (40), 4484−4488.

(28) Ko, K. T.; Jung, M. H.; He, Q.; Lee, J. H.; Woo, C. S.; Chu, K.; Seidel, J.; Jeon, B. G.; Oh, Y. S.; Kim, K. H.; Liang, W. I.; Chen, H. J.; Chu, Y. H.; Jeong, Y. H.; Ramesh, R.; Park, J. H.; Yang, C. H. Concurrent Transition of Ferroelectric and Magnetic Ordering near Room Temperature. *Nat. Commun.* **2011**, *2*, 567.

(29) Ravindran, P.; Delin, A.; Johansson, B.; Eriksson, O.; Wills, J. Electronic Structure, Chemical Bonding, and Optical Properties of Ferroelectric and Antiferroelectric $NaNO_2$. *Phys. Rev. B* **1999**, *59* (3), 1776.

(30) Horiuchi, S.; Tokura, Y. Organic Ferroelectrics. *Nat. Mater.* **2008**, *7* (5), 357−366.

(31) Gerlich, A.; Su, P.; Yamamoto, M.; North, T. Material Flow and Intermixing During Dissimilar Friction Stir Welding. *Sci. Technol. Weld. Joining* **2008**, *13* (3), 254−264.

(32) Bhadeshia, H.; DebRoy, T. Critical Assessment: Friction Stir Welding of Steels. *Sci. Technol. Weld. Joining* **2009**, *14* (3), 193−196.

(33) Harman, G. G. *Wire Bonding in Microelectronics: Materials, Processes, Reliability, and Yield;* McGraw-Hill: New York, 1997; Vol. *21*.

(34) Lancaster, J. F. *Metallurgy of Welding;* Abington Publishing: Cambridge, U.K., 1999.

(35) Peng, P.; Liu, L.; Gerlich, A. P.; Hu, A.; Zhou, Y. N. Self-Oriented Nanojoining of Silver Nanowires Via Surface Selective Activation. *Part. Part. Syst. Charact.* **2013**, *30* (5), 420−426.

(36) Dong, L.; Tao, X.; Zhang, L.; Zhang, X.; Nelson, B. J.; Nanorobotic Spot. Welding: Controlled Metal Deposition with Attogram Precision from Copper-Filled Carbon Nanotubes. *Nano Lett.* **2007**, *7* (1), 58−63.

(37) Chen, C.; Yan, L.; Kong, E. S.-W.; Zhang, Y. Ultrasonic Nanowelding of Carbon Nanotubes to Metal Electrodes. *Nanotechnology* **2006**, *17* (9), 2192.

DOI: 10.1021/acsami.5b02134
ACS Appl. Mater. Interfaces 2015, 7, 12597−12618

(38) Gao, F.; Gu, Z. Nano-Soldering of Magnetically Aligned Three-Dimensional Nanowire Networks. *Nanotechnology* **2010**, *21* (11), 115604.
(39) Cui, Q.; Gao, F.; Mukherjee, S.; Gu, Z. Joining and Interconnect Formation of Nanowires and Carbon Nanotubes for Nanoelectronics and Nanosystems. *Small* **2009**, *5* (11), 1246−1257.
(40) Garnett, E. C.; Cai, W. S.; Cha, J. J.; Mahmood, F.; Connor, S. T.; Christoforo, M. G.; Cui, Y.; McGehee, M. D.; Brongersma, M. L. Self-Limited Plasmonic Welding of Silver Nanowire Junctions. *Nat. Mater.* **2012**, *11* (3), 241−249.
(41) Pereira, Z.; Da Silva, E. Cold Welding of Gold and Silver Nanowires: A Molecular Dynamics Study. *J. Phys. Chem. C* **2011**, *115* (46), 22870−22876.
(42) Hu, A.; Peng, P.; Alarifi, H.; Zhang, X.; Guo, J.; Zhou, Y.; Duley, W. Femtosecond Laser Welded Nanostructures and Plasmonic Devices. *J. Laser Appl.* **2012**, *24* (4), 042001 DOI: 10.2351/1.3695174.
(43) Couchman, P. R.; Jesser, W. A. Thermodynamic Theory of Size Dependence of Melting Temperature in Metals. *Nature* **1977**, *269*, 481−483.
(44) Nanda, K.; Sahu, S.; Behera, S. Liquid-Drop Model for the Size-Dependent Melting of Low-Dimensional Systems. *Phys. Rev. A* **2002**, *66* (1), 013208.
(45) Alarifi, H.; Hu, A. M.; Yavuz, M.; Zhou, Y. N. Silver Nanoparticle Paste for Low-Temperature Bonding of Copper. *J. Electron. Mater.* **2011**, *40* (6), 1394−1402.
(46) Bai, G. Low-Temperature Sintering of Nanoscale Silver Paste for Semiconductor Device Interconnection. Ph.D. Dissertation, Virginia Polytechnic Institute and State University, 2005.
(47) Kähler, J.; Stranz, A.; Waag, A.; Peiner, E. Thermoelectric Coolers with Sintered Silver Interconnects. *J. Electron. Mater.* **2014**, *43* (6), 2397−2404.
(48) Maruyama, M.; Matsubayashi, R.; Iwakuro, H.; Isoda, S.; Komatsu, T. Silver Nanosintering: A Lead-Free Alternative to Soldering. *Appl. Phys. A: Mater. Sci. Process.* **2008**, *93* (2), 467−470.
(49) Mei, Y.; Chen, G.; Cao, Y.; Li, X.; Han, D.; Chen, X. Simplification of Low-Temperature Sintering Nanosilver for Power Electronics Packaging. *J. Electron. Mater.* **2013**, *42* (6), 1209−1218.
(50) Yan, J. F.; Zou, G. S.; Hu, A. M.; Zhou, Y. N. Preparation of Pvp Coated Cu Nps and the Application for Low-Temperature Bonding. *J. Mater. Chem.* **2011**, *21* (40), 15981−15986.
(51) Watanabe, R.; Ishizaki, T. Enhancement of Pressure-Free Bonding with Cu Particles by the Addition of Cu−Ni Alloy Nanoparticles. *J. Mater. Chem. C* **2014**, *2* (18), 3542−3548.
(52) Kahler, J.; Heuck, N.; Wagner, A.; Stranz, A.; Peiner, E.; Waag, A. Sintering of Copper Particles for Die Attach. *IEEE Trans. Compon., Packag., Manuf. Technol.* **2012**, *2* (10), 1587−1591.
(53) Bakhishev, T.; Subramanian, V. Investigation of Gold Nanoparticle Inks for Low-Temperature Lead-Free Packaging Technology. *J. Electron. Mater.* **2009**, *38* (12), 2720−2725.
(54) Lu, C.; Lin, Y.; Wang, K.; Dai, M.; Liu, C.; Liao, L.; Chien, H.; Chen, Y. Capacitor Discharge Sintering with Silver-Nickel Nano-Composite in the Interconnection of Thermoelectric Generators. In *9th IEEE International Conference on Nano/Micro Engineered and Molecular Systems (NEMS)*, IEEE: New York, 2014; pp 370−373.
(55) Siow, K. S. Mechanical Properties of Nano-Silver Joints as Die Attach Materials. *J. Alloys Compd.* **2012**, *514*, 6−19.
(56) Vitos, L.; Ruban, A.; Skriver, H. L.; Kollar, J. The Surface Energy of Metals. *Surf. Sci.* **1998**, *411* (1), 186−202.
(57) Ouyang, G.; Tan, X.; Yang, G. Thermodynamic Model of the Surface Energy of Nanocrystals. *Phys. Rev. B* **2006**, *74* (19), 195408.
(58) Zhu, Y.; Lian, J.; Jiang, Q. Modeling of the Melting Point, Debye Temperature, Thermal Expansion Coefficient, and the Specific Heat of Nanostructured Materials. *J. Phys. Chem. C* **2009**, *113* (39), 16896−16900.
(59) Chernyshev, A. Effect of Nanoparticle Size on the Onset Temperature of Surface Melting. *Mater. Lett.* **2009**, *63* (17), 1525−1527.
(60) Qi, W.; Wang, M.; Size. and Shape Dependent Melting Temperature of Metallic Nanoparticles. *Mater. Chem. Phys.* **2004**, *88* (2), 280−284.
(61) Alarifi, H. A.; Atiş, M.; Ozdogan, C.; Hu, A.; Yavuz, M.; Zhou, Y. N. Determination of Complete Melting and Surface Premelting Points of Silver Nanoparticles by Molecular Dynamics Simulation. *J. Phys. Chem. C* **2013**, *117* (23), 12289−12298.
(62) Kuzenkova, M.; Kislyi, P.; Grabchuk, B.; Bodnaruk, N. The Structure and Properties of Sintered Boron Carbide. *J. Less-Common Met.* **1979**, *67* (1), 217−223.
(63) Lu, K. Sintering of Nanoceramics. *Int. Mater. Rev.* **2008**, *53* (1), 21−38.
(64) Mayo, M.; Hague, D.; Chen, D.-J. Processing Nanocrystalline Ceramics for Applications in Superplasticity. *Mater. Sci. Eng., A* **1993**, *166* (1), 145−159.
(65) Risbud, S. H.; Mukherjee, A.; Kim, M.; Bow, J.; Holl, R. Retention of Nanostructure in Aluminium Oxide by Very Rapid Sintering at 1150 C. *J. Mater. Res.* **1995**, *10* (2), 237−239.
(66) Fang, Z.; Wang, H. Densification and Grain Growth During Sintering of Nanosized Particles. *Int. Mater. Rev.* **2008**, *53* (6), 326−352.
(67) Guo, J.; Xu, C.; Hu, A.; Oakes, K.; Sheng, F.; Shi, Z.; Dai, J.; Jin, Z. Sintering Dynamics and Thermal Stability of Novel Configurations of Ag Clusters. *J. Phys. Chem. Solids* **2012**, *73* (11), 1350−1357.
(68) Guo, J.; Xu, C.; Hu, A.; Shi, Z.; Sheng, F.; Dai, J.; Li, Z. Welding of Gold Nanowires with Different Joining Procedures. *J. Nanopart. Res.* **2012**, *14* (2), 1−12.
(69) Marzbanrad, E.; Hu, A.; Zhao, B.; Zhou, Y. Room Temperature Nanojoining of Triangular and Hexagonal Silver Nanodisks. *J. Phys. Chem. C* **2013**, *117* (32), 16665−16676.
(70) Ding, L.; Davidchack, R. L.; Pan, J. A Molecular Dynamics Study of Sintering between Nanoparticles. *Comput. Mater. Sci.* **2009**, *45* (2), 247−256.
(71) Searcy, A. W. Driving Force for Sintering of Particles with Anisotropic Surface Energies. *J. Am. Ceram. Soc.* **1985**, *68* (10), 267−268.
(72) Wakai, F.; Shinoda, Y. Anisotropic Sintering Stress for Sintering of Particles Arranged in Orthotropic Symmetry. *Acta Mater.* **2009**, *57* (13), 3955−3964.
(73) German, R. M. Sintering Theory and Practice. In *Sintering Theory and Practice;* Wiley-VCH: Weinheim, Germany, 1996 pp. 568. ISBN 978-0-471-05786-4.
(74) Coble, R. Sintering Crystalline Solids. I. Intermediate and Final State Diffusion Models. *J. Appl. Phys.* **1961**, *32*, 787.
(75) Ch'ng, H.; Pan, J. Sintering of Particles of Different Sizes. *Acta Mater.* **2007**, *55* (3), 813−824.
(76) Schwarzbauer, H.; Kuhnert, R. Novel Large Area Joining Technique for Improved Power Device Performance. In *Conference Record of the 1989 IEEE Industry Applications Society Annual Meeting;* IEEE: New York, 1989; pp 1348−1351.
(77) Morisada, Y.; Nagaoka, T.; Fukusumi, M.; Kashiwagi, Y.; Yamamoto, M.; Nakamoto, M. A Low-Temperature Bonding Process Using Mixed Cu−Ag Nanoparticles. *J. Electron. Mater.* **2010**, *39* (8), 1283−1288.
(78) Provance, J.; Allison, K. *Particle Size Effects on Viscosity of Silver Pastes: A Manufacturer's View;* Ferro Corp.: Santa Barbara, CA, 1983.
(79) Rane, S.; Seth, T.; Phatak, G.; Amalnerkar, D.; Das, B. Influence of Surfactants Treatment on Silver Powder and Its Thick Films. *Mater. Lett.* **2003**, *57* (20), 3096−3100.
(80) Lin, J.; Wang, C. Effects of Surfactant Treatment of Silver Powder on the Rheology of Its Thick-Film Paste. *Mater. Chem. Phys.* **1996**, *45* (2), 136−144.
(81) Jørgensen, M.; Hagemann, O.; Alstrup, J.; Krebs, F. C. Thermo-Cleavable Solvents for Printing Conjugated Polymers: Application in Polymer Solar Cells. *Sol. Energy Mater. Sol. Cells* **2009**, *93* (4), 413−421.
(82) Peng, P.; Hu, A. M.; Huang, H.; Gerlich, A. P.; Zhao, B. X.; Zhou, Y. N. Room-Temperature Pressureless Bonding with Silver Nanowire Paste: Towards Organic Electronic and Heat-Sensitive

Functional Devices Packaging. *J. Mater. Chem.* **2012**, *22* (26), 12997−13001.
(83) Luo, W.; Hu, W.; Xiao, S. Size Effect on the Thermodynamic Properties of Silver Nanoparticles. *J. Phys. Chem. C* **2008**, *112* (7), 2359−2369.
(84) Alarifi, H.; Atis, M.; Özdoğan, C.; Hu, A.; Yavuz, M.; Zhou, Y. Molecular Dynamics Simulation of Sintering and Surface Premelting of Silver Nanoparticles. *Mater. Trans.* **2013**, *54* (6), 884−889.
(85) Allen, M.; Alastalo, A.; Suhonen, M.; Mattila, T.; Leppaniemi, J.; Seppa, H. Contactless Electrical Sintering of Silver Nanoparticles on Flexible Substrates. *IEEE Trans. Microwave Theory Tech.* **2011**, *59* (5), 1419−1429.
(86) Mei, Y.; Cao, Y.; Chen, G.; Li, X.; Lu, G.-Q.; Chen, X. Rapid Sintering Nanosilver Joint by Pulse Current for Power Electronics Packaging. *IEEE Trans. Device Mater. Reliab.* **2013**, *13* (1), 258−265.
(87) Ide, E.; Angata, S.; Hirose, A.; Kobayashi, K. F. Metal-Metal Bonding Process Using Ag Metallo-Organic Nanoparticles. *Acta Mater.* **2005**, *53* (8), 2385−2393.
(88) Hu, A.; Guo, J.; Alarifi, H.; Patane, G.; Zhou, Y.; Compagnini, G.; Xu, C. Low Temperature Sintering of Ag Nanoparticles for Flexible Electronics Packaging. *Appl. Phys. Lett.* **2010**, *97* (15), 153117.
(89) Bai, J. G.; Calata, J. N.; Lei, G. Y.; Lu, G. Q. Thermomechanical Reliability of Low-Temperature Sintered Silver Die-Attachment. In *10th Intersociety Conference on Thermal and Thermomechanical Phenomena in Electronics Systems, 2006 Proceedings ;* IEEE: New York, 2006; Vols. *1*−*2*, pp 1126−1130
(90) Bai, J. G.; Lu, G.-Q. Thermomechanical Reliability of Low-Temperature Sintered Silver Die Attached SiC Power Device Assembly. *IEEE Trans. Device Mater. Reliab.* **2006**, *6* (3), 436−441.
(91) Yan, J.; Zou, G.; Wu, A.; Ren, J.; Hu, A.; Zhou, Y. N. Improvement of Bondability by Depressing the Inhomogeneous Distribution of Nanoparticles in a Sintering Bonding Process with Silver Nanoparticles. *J. Electron. Mater.* **2012**, *41* (7), 1924−1930.
(92) Yan, J.; Zou, G.; Wu, A.; Ren, J.; Yan, J.; Hu, A.; Liu, L.; Zhou, Y. N. Effect of PVP on the Low Temperature Bonding Process Using Polyol Prepared Ag Nanoparticle Paste for Electronic Packaging Application. *J. Phys: Conf. Ser.* **2012**, *379* (1), 012024.
(93) Yan, J.; Zou, G.; Wu, A.-p.; Ren, J.; Yan, J.; Hu, A.; Zhou, Y. Pressureless Bonding Process Using Ag Nanoparticle Paste for Flexible Electronics Packaging. *Scr. Mater.* **2012**, *66* (8), 582−585.
(94) Zhang, Z.; Lu, G.-Q. Pressure-Assisted Low-Temperature Sintering of Silver Paste as an Alternative Die-Attach Solution to Solder Reflow. *IEEE Trans. Electron. Packag. Manuf.* **2002**, *25* (4), 279−283.
(95) Morita, T.; Ide, E.; Yasuda, Y.; Hirose, A.; Kobayashi, K. Study of Bonding Technology Using Silver Nanoparticles. *Jpn. J. Appl. Phys.* **2008**, *47*, 6615.
(96) Wang, S.; Li, M.; Kim, J., Twin-Induced Ultra-High Thermal Conductivity of Sintering Ag Nanoparticles for High Power Density Electronic Packaging. *15th International Conference on Electronic Packaging Technology (ICEPT);* IEEE: New York, 2014; pp 163−166.
(97) Lei, T. G.; Calata, J. N.; Lu, G.-Q.; Chen, X.; Luo, S. Low-Temperature Sintering of Nanoscale Silver Paste for Attaching Large-Area (> 100 mm^2) Chips. *IEEE Trans. Compon. Packag. Technol.* **2010**, *33* (1), 98−104.
(98) Egelkraut, S.; Frey, L.; Knoerr, M.; Schletz, A., Evolution of Shear Strength and Microstructure of Die Bonding Technologies for High Temperature Applications During Thermal Aging. *12th Electronics Packaging Technology Conference (EPTC);* IEEE: New York, 2010; pp 660−667.
(99) Knoerr, M.; Kraft, S.; Schletz, A., Reliability Assessment of Sintered Nano-Silver Die Attachment for Power Semiconductors. *12th Electronics Packaging Technology Conference (EPTC);* IEEE: New York, 2010; pp 56−61.
(100) Knoerr, M.; Schletz, A. Power Semiconductor Joining through Sintering of Silver Nanoparticles: Evaluation of Influence of Parameters Time, Temperature and Pressure on Density, Strength and Reliability. *6th International Conference on Integrated Power Electronics Systems (CIPS);* IEEE: New York, 2010; pp 1−6.
(101) Morisada, Y.; Nagaoka, T.; Fukusumi, M.; Kashiwagi, Y.; Yamamoto, M.; Nakamoto, M.; Kakiuchi, H.; Yoshida, Y. A Low-Temperature Pressureless Bonding Process Using a Trimodal Mixture System of Ag Nanoparticles. *J. Electron. Mater.* **2011**, *40* (12), 2398−2402.
(102) Hirose, A.; Tatsumi, H.; Takeda, N.; Akada, Y.; Ogura, T.; Ide, E.; Morita, T. A Novel Metal-to-Metal Bonding Process through in-Situ Formation of Ag Nanoparticles Using Ag2O Microparticles. *J. Phys: Conf. Ser.* **2009**, *165* (1), 012074.
(103) Yasuda, Y.; Tokoo, N.; Morita, T.; Suzuki, K. Reliability of Sintered Silver Layer Obtained Using Silver-Oxide Paste in Power Cycling Test. *Jpn. J. Appl. Phys.* **2015**, *54* (1), 010302.
(104) Suzuki, Y.; Ogura, T.; Takahashi, M.; Hirose, A. Low-Current Resistance Spot Welding of Pure Copper Using Silver Oxide Paste. *Mater. Charact.* **2014**, *98*, 186−192.
(105) Sakamoto, S.; Nagao, S.; Suganuma, K. Thermal Fatigue of Ag Flake Sintering Die-Attachment for Si/SiC Power Devices. *J. Mater. Sci.: Mater. Electron.* **2013**, *24* (7), 2593−2601.
(106) Peng, P.; Hu, A. M.; Zhao, B. X.; Gerlich, A. P.; Zhou, Y. N. Reinforcement of Ag Nanoparticle Paste with Nanowires for Low Temperature Pressureless Bonding. *J. Mater. Sci.* **2012**, *47* (19), 6801−6811.
(107) Jiang, H., Synthesis of Tin, Silver and Their Alloy Nanoparticles for Lead-Free Interconnect Applications. Ph.D. Dissertation, Georgia Institute of Technology, 2008.
(108) Yan, J.; Zou, G.; Wu, A.; Ren, J.; Hu, A.; Zhou, Y. N. Polymer-Protected Cu-Ag Mixed Nps for Low-Temperature Bonding Application. *J. Electron. Mater.* **2012**, *41* (7), 1886−1892.
(109) Kim, S. J.; Stach, E. A.; Handwerker, C. A. Fabrication of Conductive Interconnects by Ag Migration in Cu−Ag Core-Shell Nanoparticles. *Appl. Phys. Lett.* **2010**, *96* (14), 144101.
(110) Satoh, T.; Ishizaki, T. Enhanced Pressure-Free Bonding Using Mixture of Cu and Nio Nanoparticles. *J. Alloys Compd.* **2015**, *629*, 118−123.
(111) Shu, Y.; Rajathurai, K.; Gao, F.; Cui, Q.; Gu, Z. Synthesis and Thermal Properties of Low Melting Temperature Tin/Indium (Sn/in) Lead-Free Nanosolders and Their Melting Behavior in a Vapor Flux. *J. Alloys Compd.* **2015**, *626*, 391−400.
(112) Watanabe, R.; Ishizaki, T. High-Strength Pressure-Free Bonding Using Cu and Ni-Sn Nanoparticles. *Part. Part. Syst. Charact.* **2014**, *31* (6), 699−705.
(113) Siow, K. Are Sintered Silver Joints Ready for Use as Interconnect Material in Microelectronic Packaging? *J. Electron. Mater.* **2014**, *43* (4), 947−961.
(114) Manikam, V. R.; Cheong, K. Y. Die Attach Materials for High Temperature Applications: A Review. *IEEE Trans. Compon., Packag., Manuf. Technol.* **2011**, *1* (4), 457−478.
(115) Kisiel, R.; Szczepański, Z. Die-Attachment Solutions for SiC Power Devices. *Microelectron. Reliab.* **2009**, *49* (6), 627−629.
(116) Chen, G.; Han, D.; Mei, Y.-H.; Cao, X.; Wang, T.; Chen, X.; Lu, G.-Q. Transient Thermal Performance of Igbt Power Modules Attached by Low-Temperature Sintered Nanosilver. *IEEE Trans. Device Mater. Reliab.* **2012**, *12* (1), 124−132.
(117) Chen, G.; Yu, L.; Mei, Y.-H.; Li, X.; Chen, X.; Lu, G.-Q. Reliability Comparison between Sac305 Joint and Sintered Nanosilver Joint at High Temperatures for Power Electronic Packaging. *J. Mater. Process. Technol.* **2014**, *214* (9), 1900−1908.
(118) Mei, Y.-H.; Cao, Y.; Chen, G.; Li, X.; Lu, G.-Q.; Chen, X. Characterization and Reliability of Sintered Nanosilver Joints by a Rapid Current-Assisted Method for Power Electronics Packaging. *IEEE Trans. Device Mater. Reliab.* **2014**, *14* (1), 262−267.
(119) Mei, Y.; Lian, J.; Chen, X.; Chen, G.; Li, X.; Lu, G. Thermo-Mechanical Reliability of Double-Sided IGBT Assembly Bonded by Sintered Nanosilver. *IEEE Trans. Device Mater. Reliab.* **2014**, *14* (1), 194−202.
(120) Chen, G.; Zhang, Z.-S.; Mei, Y.-H.; Li, X.; Yu, D.-J.; Wang, L.; Chen, X. Applying Viscoplastic Constitutive Models to Predict Ratcheting Behavior of Sintered Nanosilver Lap-Shear Joint. *Mech. Mater.* **2014**, *72*, 61−71.

DOI: 10.1021/acsami.5b02134
ACS Appl. Mater. Interfaces 2015, 7, 12597−12618

(121) Chen, G.; Yu, L.; Mei, Y.; Li, X.; Chen, X.; Lu, G.-Q. Uniaxial Ratcheting Behavior of Sintered Nanosilver Joint for Electronic Packaging. *Mater. Sci. Eng., A* **2014**, *591*, 121−129.
(122) Li, X.; Chen, G.; Wang, L.; Mei, Y.-H.; Chen, X.; Lu, G.-Q. Creep Properties of Low-Temperature Sintered Nano-Silver Lap Shear Joints. *Mater. Sci. Eng., A* **2013**, *579*, 108−113.
(123) Chen, G.; Zhang, Z.-S.; Mei, Y.-H.; Li, X.; Lu, G.-Q.; Chen, X. Ratcheting Behavior of Sandwiched Assembly Joined by Sintered Nanosilver for Power Electronics Packaging. *Microelectron. Reliab.* **2013**, *53* (4), 645−651.
(124) Li, X.; Chen, G.; Chen, X.; Lu, G.-Q.; Wang, L.; Mei, Y.-H. High Temperature Ratcheting Behavior of Nano-Silver Paste Sintered Lap Shear Joint under Cyclic Shear Force. *Microelectron. Reliab.* **2013**, *53* (1), 174−181.
(125) Guofeng Bai, J.; Yin, J.; Zhang, Z.; Lu, G.-Q.; van Wyk, J. D. High-Temperature Operation of SiC Power Devices by Low-Temperature Sintered Silver Die-Attachment. *IEEE Trans. Adv. Packag.* **2007**, *30* (3), 506−510.
(126) Herboth, T.; Guenther, M.; Fix, A.; Wilde, J. Failure Mechanisms of Sintered Silver Interconnections for Power Electronic Applications. *IEEE 63rd Electronic Components and Technology Conference (ECTC);* IEEE: New York, 2013; pp 1621−1627.
(127) Jiang, L. Thermo-Mechanical Reliability of Sintered-Silver Joint Versus Lead-Free Solder for Attaching Large-Area Devices. Ph.D. Dissertation, Virginia Polytechnic Institute and State University, 2010.
(128) Ogura, H.; Maruyama, M.; Matsubayashi, R.; Ogawa, T.; Nakamura, S.; Komatsu, T.; Nagasawa, H.; Ichimura, A.; Isoda, S. Carboxylate-Passivated Silver Nanoparticles and Their Application to Sintered Interconnection: A Replacement for High Temperature Lead-Rich Solders. *J. Electron. Mater.* **2010**, *39* (8), 1233−1240.
(129) Zou, G.; Yan, J.; Mu, F.; Wu, A.; Ren, J.; Hu, A.; Zhou, Y. Low Temperature Bonding of Cu Metal through Sintering of Ag Nanoparticles for High Temperature Electronic Application. *Open Surf. Sci. J.* **2011**, *3*, 70−75.
(130) Lee, M. Y.; Lee, W. J.; Roy, A. K.; Lee, K. S.; Park, S. Y.; Lee, J.-H.; In, I. Room-Temperature Sinterable Silver Nanoparticle Ink with Low-Molecular-Weight Poly (N-Vinylpyrrolidone) Ligand. *Chem. Lett.* **2013**, *42* (3), 232−234.
(131) Durairaj, R.; Ashayer, R.; Kotadia, H. R.; Haria, N.; Lorenz, C.; Mokhtari, O.; Mannan, S. H. Pressure Free Sintering of Silver Nanoparticles to Silver Substrate Using Weakly Binding Ligands. *12th IEEE Conference on Nanotechnology (IEEE-NANO);* IEEE: New York, 2012; pp 1−4.
(132) Le Henaff, F.; Azzopardi, S.; Delétage, J.-Y.; Woirgard, E.; Bontemps, S.; Joguet, J. A Preliminary Study on the Thermal and Mechanical Performances of Sintered Nano-Scale Silver Die-Attach Technology Depending on the Substrate Metallization. *Microelectron. Reliab.* **2012**, *52* (9), 2321−2325.
(133) Morita, T.; Yasuda, Y.; Ide, E.; Akada, Y.; Hirose, A. Bonding Technique Using Micro-Scaled Silver-Oxide Particles for in-Situ Formation of Silver Nanoparticles. *Mater. Trans.* **2008**, *49* (12), 2875.
(134) Wang, T.; Chen, X.; Lu, G.-Q.; Lei, G.-Y. Low-Temperature Sintering with Nano-Silver Paste in Die-Attached Interconnection. *J. Electron. Mater.* **2007**, *36* (10), 1333−1340.
(135) Fu, S.; Mei, Y.; Lu, G.-Q.; Li, X.; Chen, G.; Chen, X. Pressureless Sintering of Nanosilver Paste at Low Temperature to Join Large Area ($\geq$ 100mm ^{2}) Power Chips for Electronic Packaging. *Mater. Lett.* **2014**, *128*, 42−45.
(136) Wang, S.; Ji, H.; Li, M.; Wang, C. Fabrication of Interconnects Using Pressureless Low Temperature Sintered Ag Nanoparticles. *Mater. Lett.* **2012**, *85*, 61−63.
(137) Suganuma, K.; Sakamoto, S.; Kagami, N.; Wakuda, D.; Kim, K.-S.; Nogi, M. Low-Temperature Low-Pressure Die Attach with Hybrid Silver Particle Paste. *Microelectron. Reliab.* **2012**, *52* (2), 375−380.
(138) Wakuda, D.; Hatamura, M.; Suganuma, K. Novel Method for Room Temperature Sintering of Ag Nanoparticle Paste in Air. *Chem. Phys. Lett.* **2007**, *441* (4), 305−308.
(139) Wakuda, D.; Kim, K.-S.; Suganuma, K. Ag Nanoparticle Paste Synthesis for Room Temperature Bonding. *IEEE Trans. Compon. Packag. Technol.* **2010**, *33* (2), 437−442.
(140) Wakuda, D.; Kim, K.-S.; Suganuma, K. Room Temperature Sintering of Ag Nanoparticles by Drying Solvent. *Scr. Mater.* **2008**, *59* (6), 649−652.
(141) Wakuda, D.; Kim, K.-S.; Suganuma, K. Room-Temperature Sintering Process of Ag Nanoparticle Paste. *IEEE Trans. Compon. Packag. Technol.* **2009**, *32* (3), 627−632.
(142) Li, W.-H.; Lin, P.-S.; Chen, C.-N.; Dong, T.-Y.; Tsai, C.-H.; Kung, W.-T.; Song, J.-M.; Chiu, Y.-T.; Yang, P.-F. Low-Temperature Cu-to-Cu Bonding Using Silver Nanoparticles Stabilised by Saturated Dodecanoic Acid. *Mater. Sci. Eng., A* **2014**, *613*, 372−378.
(143) Peng, P.; Hu, A.; Gerlich, A.; Liu, Y.-G.; Zhou, Y. Self-Generated Local Heating Induced Nanojoining for Room Temperature Pressureless Flexible Electronic Packaging. *Sci. Rep.* **2015**, *5*, 9282 DOI: 10.1038/srep09282.
(144) Lee, M. Y.; Lee, J. Y.; Lee, W. J.; Kim, S. Y.; Park, Y. H.; Mosaiab, T.; Park, S. Y.; In, I. Photocatalytic Effect of Tio 2 Nanoparticles on Room-Temperature Sinterable Silver Nanoparticle Ink with Poly (N-Vinylpyrrolidone) Ligand. *Chem. Lett.* **2013**, *42* (6), 649−650.
(145) Zuruzi, A. S.; Siow, K. S. Electrical Conductivity of Porous Silver Made from Sintered Nanoparticles. *Electron. Mater. Lett.* **2015**, *11* (2), 308−314.
(146) Scola, J.; Tassart, X.; Vilar, C.; Jomard, F.; Dumas, E.; Veniaminova, Y.; Boullay, P.; Gascoin, S. Microstructure and Electrical Resistance Evolution During Sintering of a Ag Nanoparticle Paste. *J. Phys. D: Appl. Phys.* **2015**, *48* (14), 145302.
(147) Zhang, R.; Moon, K.-s.; Lin, W.; Wong, C. Preparation of Highly Conductive Polymer Nanocomposites by Low Temperature Sintering of Silver Nanoparticles. *J. Mater. Chem.* **2010**, *20* (10), 2018−2023.
(148) Pulkkinen, P.; Shan, J.; Leppänen, K.; Känsäkoski, A.; Laiho, A.; Järn, M.; Tenhu, H. Poly (Ethylene Imine) and Tetraethylenepentamine as Protecting Agents for Metallic Copper Nanoparticles. *ACS Appl. Mater. Interfaces* **2009**, *1* (2), 519−525.
(149) Jiang, H.; Moon, K.-s.; Li, Y.; Wong, C. Surface Functionalized Silver Nanoparticles for Ultrahigh Conductive Polymer Composites. *Chem. Mater.* **2006**, *18* (13), 2969−2973.
(150) Riva, R.; Buttay, C.; Allard, B.; Bevilacqua, P. Migration Issues in Sintered-Silver Die Attaches Operating at High Temperature. *Microelectron. Reliab.* **2013**, *53* (9), 1592−1596.
(151) Lu, G.; Yang, W.; Mei, Y.; Li, X.; Chen, G.; Chen, X. Migration of Sintered Nanosilver on Alumina (Al2O3) and Aluminum Nitride (AlN) Substrates at High Temperatures in Dry Air for Electronic Packaging. *IEEE Trans. Device Mater. Reliab.* **2014**, *14* (2), 600−606.
(152) Lu, G.-Q.; Yang, W.; Mei, Y.-H.; Li, X.; Chen, G.; Chen, X. Mechanism of Migration of Sintered Nanosilver at High Temperatures in Dry Air for Electronic Packaging. *IEEE Trans. Device Mater. Reliab.* **2014**, *14* (1), 311−317.
(153) Heersche, H. B.; Lientschnig, G.; ONeill, K.; van der Zant, H. S.; Zandbergen, H. W. In Situ Imaging of Electromigration-Induced Nanogap Formation by Transmission Electron Microscopy. *Appl. Phys. Lett.* **2007**, *91* (7), 072107−072107−3.
(154) Zhang, X.-Y.; Hu, A.; Zhang, T.; Lei, W.; Xue, X.-J.; Zhou, Y.; Duley, W. W. Self-Assembly of Large-Scale and Ultrathin Silver Nanoplate Films with Tunable Plasmon Resonance Properties. *ACS Nano* **2011**, *5* (11), 9082−9092.
(155) Liang, H.; Li, Z.; Wang, W.; Wu, Y.; Xu, H. Highly Surface-Roughened "Flower-Like" Silver Nanoparticles for Extremely Sensitive Substrates of Surface-Enhanced Raman Scattering. *Adv. Mater.* **2009**, *21* (45), 4614−4618.
(156) Zhou, W.; Hu, A.; Bai, S.; Ma, Y.; Bridges, D. Anisotropic Optical Properties of Large-Scale Aligned Silver Nanowire Films Via Controlled Coffee Ring Effects. *RSC Adv.* **2015**, *5* (49), 39103−39109.
(157) Chursanova, M.; Dzhagan, V.; Yukhymchuk, V.; Lytvyn, O.; Valakh, M. Y.; Khodasevich, I.; Lehmann, D.; Zahn, D.; Waurisch, C.; Hickey, S. Nanostructured Silver Substrates with Stable and Universal

Sers Properties: Application to Organic Molecules and Semiconductor Nanoparticles. *Nanoscale Res. Lett.* **2010**, *5* (2), 403−409.
(158) Tanyeli, I.; Nasser, H.; Es, F.; Bek, A.; Turan, R. Effect of Surface Type on Structural and Optical Properties of Ag Nanoparticles Formed by Dewetting. *Opt. Express* **2013**, *21* (105), A798−A807.
(159) McLellan, J. M.; Li, Z.-Y.; Siekkinen, A. R.; Xia, Y. The Sers Activity of a Supported Ag Nanocube Strongly Depends on Its Orientation Relative to Laser Polarization. *Nano Lett.* **2007**, *7* (4), 1013−1017.
(160) Shanmukh, S.; Jones, L.; Driskell, J.; Zhao, Y.; Dluhy, R.; Tripp, R. A. Rapid and Sensitive Detection of Respiratory Virus Molecular Signatures Using a Silver Nanorod Array Sers Substrate. *Nano Lett.* **2006**, *6* (11), 2630−2636.
(161) Peng, P.; Huang, H.; Hu, A. M.; Gerlich, A. P.; Zhou, Y. N. Functionalization of Silver Nanowire Surfaces with Copper Oxide for Surface-Enhanced Raman Spectroscopic Bio-Sensing. *J. Mater. Chem.* **2012**, *22* (31), 15495−15499.
(162) Zhang, T.; Zhang, X.-Y.; Xue, X.-J.; Wu, X.-F.; Li, C.; Hu, A. Plasmonic Properties of Welded Metal Nanoparticles. *Open Surf. Sci. J.* **2011**, *3*, 76−81.
(163) Huang, H.; Liu, L.; Peng, P.; Hu, A.; Duley, W.; Zhou, Y. Controlled Joining of Ag Nanoparticles with Femtosecond Laser Radiation. *J. Appl. Phys.* **2012**, *112* (12), 123519.
(164) Ko, S. H.; Pan, H.; Grigoropoulos, C. P.; Luscombe, C. K.; Fréchet, J. M.; Poulikakos, D. All-Inkjet-Printed Flexible Electronics Fabrication on a Polymer Substrate by Low-Temperature High-Resolution Selective Laser Sintering of Metal Nanoparticles. *Nanotechnology* **2007**, *18* (34), 345202.
(165) Hong, S.; Yeo, J.; Kim, G.; Kim, D.; Lee, H.; Kwon, J.; Lee, H.; Lee, P.; Ko, S. H. Nonvacuum, Maskless Fabrication of a Flexible Metal Grid Transparent Conductor by Low-Temperature Selective Laser Sintering of Nanoparticle Ink. *ACS Nano* **2013**, *7* (6), 5024−5031.
(166) Fukuda, K.; Sekine, T.; Kumaki, D.; Tokito, S. Profile Control of Inkjet Printed Silver Electrodes and Their Application to Organic Transistors. *ACS Appl. Mater. Interfaces* **2013**, *5* (9), 3916−3920.
(167) Chen, S.-P.; Kao, Z.-K.; Lin, J.-L.; Liao, Y.-C. Silver Conductive Features on Flexible Substrates from a Thermally Accelerated Chain Reaction at Low Sintering Temperatures. *ACS Appl. Mater. Interfaces* **2012**, *4* (12), 7064−7068.
(168) Mahajan, A.; Frisbie, C. D.; Francis, L. F. Optimization of Aerosol Jet Printing for High-Resolution, High-Aspect Ratio Silver Lines. *ACS Appl. Mater. Interfaces* **2013**, *5* (11), 4856−4864.
(169) Alshehri, A. H.; Jakubowska, M.; Młożniak, A.; Horaczek, M.; Rudka, D.; Free, C.; Carey, J. D. Enhanced Electrical Conductivity of Silver Nanoparticles for High Frequency Electronic Applications. *ACS Appl. Mater. Interfaces* **2012**, *4* (12), 7007−7010.
(170) Kang, J. S.; Kim, H. S.; Ryu, J.; Hahn, H. T.; Jang, S.; Joung, J. W. Inkjet Printed Electronics Using Copper Nanoparticle Ink. *J. Mater. Sci.: Mater. Electron.* **2010**, *21* (11), 1213−1220.
(171) Walker, S. B.; Lewis, J. A. Reactive Silver Inks for Patterning High-Conductivity Features at Mild Temperatures. *J. Am. Chem. Soc.* **2012**, *134* (3), 1419−1421.
(172) Zhang, R.; Lin, W.; Moon, K.-s.; Wong, C. Fast Preparation of Printable Highly Conductive Polymer Nanocomposites by Thermal Decomposition of Silver Carboxylate and Sintering of Silver Nanoparticles. *ACS Appl. Mater. Interfaces* **2010**, *2* (9), 2637−2645.
(173) Amoli, B. M.; Hu, A.; Zhou, N. Y.; Zhao, B. Recent Progresses on Hybrid Micro−Nano Filler Systems for Electrically Conductive Adhesives (ECAs) Applications. *J. Mater. Sci.: Mater. Electron.* **2015**, DOI: 10.1007/s10854-015-3016-1.
(174) Lee, H.-H.; Chou, K.-S.; Huang, K.-C. Inkjet Printing of Nanosized Silver Colloids. *Nanotechnology* **2005**, *16* (10), 2436.
(175) Chiolerio, A.; Maccioni, G.; Martino, P.; Cotto, M.; Pandolfi, P.; Rivolo, P.; Ferrero, S.; Scaltrito, L. Inkjet Printing and Low Power Laser Annealing of Silver Nanoparticle Traces for the Realization of Low Resistivity Lines for Flexible Electronics. *Microelectron. Eng.* **2011**, *88* (8), 2481−2483.
(176) Kim, M.-K.; Kang, H.; Kang, K.; Lee, S.-H.; Hwang, J. Y.; Moon, Y.; Moon, S.-J. Laser Sintering of Inkjet-Printed Silver Nanoparticles on Glass and Pet Substrates. *10th IEEE Conference on Nanotechnology (IEEE-NANO);* IEEE: New York, 2010; pp 520−524.
(177) Tobjörk, D.; Aarnio, H.; Pulkkinen, P.; Bollström, R.; Määttänen, A.; Ihalainen, P.; Mäkelä, T.; Peltonen, J.; Toivakka, M.; Tenhu, H. Ir-Sintering of Ink-Jet Printed Metal-Nanoparticles on Paper. *Thin Solid Films* **2012**, *520* (7), 2949−2955.
(178) Kim, H.-S.; Dhage, S. R.; Shim, D.-E.; Hahn, H. T. Intense Pulsed Light Sintering of Copper Nanoink for Printed Electronics. *Appl. Phys. A: Mater. Sci. Process.* **2009**, *97* (4), 791−798.
(179) Hösel, M.; Krebs, F. C. Large-Scale Roll-to-Roll Photonic Sintering of Flexo Printed Silver Nanoparticle Electrodes. *J. Mater. Chem.* **2012**, *22* (31), 15683−15688.
(180) Yung, K.; Gu, X.; Lee, C.; Choy, H. Ink-Jet Printing and Camera Flash Sintering of Silver Tracks on Different Substrates. *J. Mater. Process. Technol.* **2010**, *210* (15), 2268−2272.
(181) Abbel, R.; van Lammeren, T.; Hendriks, R.; Ploegmakers, J.; Rubingh, E. J.; Meinders, E. R.; Groen, W. A. Photonic Flash Sintering of Silver Nanoparticle Inks: A Fast and Convenient Method for the Preparation of Highly Conductive Structures on Foil. *MRS Commun.* **2012**, *2* (04), 145−150.
(182) Li, R.-Z.; Hu, A.; Zhang, T.; Oakes, K. D. Direct Writing on Paper of Foldable Capacitive Touch Pads with Silver Nanowire Inks. *ACS Appl. Mater. Interfaces* **2014**, *6* (23), 21721−21729.
(183) Huang, H.; Sivayoganathan, M.; Duley, W.; Zhou, Y. Efficient Localized Heating of Silver Nanoparticles by Low-Fluence Femtosecond Laser Pulses. *Appl. Surf. Sci.* **2015**, *331*, 392−398.
(184) Jiao, Z.; Huang, H.; Liu, L.; Hu, A.; Duley, W.; He, P.; Zhou, Y. Nanostructure Evolution in Joining of Al and Fe Nanoparticles with Femtosecond Laser Irradiation. *J. Appl. Phys.* **2014**, *115* (13), 134305.
(185) Jiao, Z.; Sivayoganathan, M.; Duley, W. W.; He, P.; Zhou, Y. N. Formation and Characterization of Femtosecond-Laser-Induced Subcluster Segregated Nanoalloys. *J. Phys. Chem. C* **2014**, *118* (42), 24746−24751.
(186) Son, Y.; Lim, T. W.; Yeo, J.; Ko, S. H.; Yang, D.-Y. Fabrication of Nano-Scale Conductors by Selective Femtosecond Laser Sintering of Metal Nanoparticles. *10th IEEE Conference on Nanotechnology (IEEE-NANO);* IEEE: New York, 2010; pp 390−393.
(187) Liu, L.; Peng, P.; Hu, A.; Zou, G.; Duley, W.; Zhou, Y. N. Highly Localized Heat Generation by Femtosecond Laser Induced Plasmon Excitation in Ag Nanowires. *Appl. Phys. Lett.* **2013**, *102* (7), 073107.
(188) Lin, L.; Huang, H.; Sivayoganathan, M.; Liu, L.; Zou, G.; Duley, W.; Zhou, Y. Assembly of Silver Nanoparticles on Nanowires into Ordered Nanostructures with Femtosecond Laser Radiation. *Appl. Opt.* **2015**, *54* (9), 2524−2531.
(189) Liu, L.; Huang, H.; Hu, A.; Zou, G.; Quintino, L.; Zhou, Y. Nano Brazing of Pt-Ag Nanoparticles under Femtosecond Laser Irradiation. *Nano-Micro Lett.* **2013**, *5* (2), 88−92.
(190) Huang, H.; Sivayoganathan, M.; Duley, W.; Zhou, Y. High Integrity Interconnection of Silver Submicron/Nanoparticles on Silicon Wafer by Femtosecond Laser Irradiation. *Nanotechnology* **2015**, *26* (2), 025303.
(191) Krzanowski, J. E. A Transmission Electron Microscopy Study of Ultrasonic Wire Bonding. *Proceedings, 39th Electronic Components Conference;* IEEE: New York, 1989; pp 450−455.
(192) Li, L.; Nagai, K.; Yin, F. Progress in Cold Roll Bonding of Metals. *Sci. Technol. Adv. Mater.* **2008**, *9* (2), 023001.
(193) Ma, Q.; Wang, Z.; Zhong, Y. The Mechanism of Faults Originating from Inclusions in the Plastic Deformation Processes of Heavy Forging. *J. Mater. Process. Technol.* **2002**, *123* (1), 61−66.
(194) Shigematsu, I.; Kwon, Y.-J.; Suzuki, K.; Imai, T.; Saito, N. Joining of 5083 and 6061 Aluminum Alloys by Friction Stir Welding. *J. Mater. Sci. Lett.* **2003**, *22* (5), 353−356.
(195) Nandan, R.; DebRoy, T.; Bhadeshia, H. Recent Advances in Friction-Stir Welding−Process, Weldment Structure and Properties. *Prog. Mater. Sci.* **2008**, *53* (6), 980−1023.

DOI: 10.1021/acsami.5b02134
ACS Appl. Mater. Interfaces 2015, 7, 12597−12618

(196) Tokuno, T.; Nogi, M.; Karakawa, M.; Jiu, J.; Nge, T. T.; Aso, Y.; Suganuma, K. Fabrication of Silver Nanowire Transparent Electrodes at Room Temperature. *Nano Res.* **2011**, *4* (12), 1215−1222.
(197) Magdassi, S.; Grouchko, M.; Berezin, O.; Kamyshny, A. Triggering the Sintering of Silver Nanoparticles at Room Temperature. *ACS Nano* **2010**, *4* (4), 1943−1948.
(198) Layani, M.; Grouchko, M.; Shemesh, S.; Magdassi, S. Conductive Patterns on Plastic Substrates by Sequential Inkjet Printing of Silver Nanoparticles and Electrolyte Sintering Solutions. *J. Mater. Chem.* **2012**, *22* (29), 14349−14352.
(199) Layani, M.; Magdassi, S. Flexible Transparent Conductive Coatings by Combining Self-Assembly with Sintering of Silver Nanoparticles Performed at Room Temperature. *J. Mater. Chem.* **2011**, *21* (39), 15378−15382.
(200) Tang, Y.; He, W.; Zhou, G.; Wang, S.; Yang, X.; Tao, Z.; Zhou, J. A New Approach Causing the Patterns Fabricated by Silver Nanoparticles to Be Conductive without Sintering. *Nanotechnology* **2012**, *23* (35), 355304.
(201) Grouchko, M.; Kamyshny, A.; Mihailescu, C. F.; Anghel, D. F.; Magdassi, S. Conductive Inks with a "Built-in" Mechanism That Enables Sintering at Room Temperature. *ACS Nano* **2011**, *5* (4), 3354−3359.
(202) Hu, L.; Kim, H. S.; Lee, J.-Y.; Peumans, P.; Cui, Y. Scalable Coating and Properties of Transparent, Flexible, Silver Nanowire Electrodes. *ACS Nano* **2010**, *4* (5), 2955−2963.
(203) Ni, C.-J.; Hong, F. C.-N. Electroless Nanowelding of Silver Nanowires at Room Temperature. *RSC Adv.* **2014**, *4* (76), 40330−40338.
(204) Gu, Z.; Chen, Y.; Gracias, D. H. Surface Tension Driven Self-Assembly of Bundles and Networks of 200 Nm Diameter Rods Using a Polymerizable Adhesive. *Langmuir* **2004**, *20* (26), 11308−11311.
(205) Henzie, J.; Andrews, S. C.; Ling, X. Y.; Li, Z.; Yang, P. Oriented Assembly of Polyhedral Plasmonic Nanoparticle Clusters. *Proc. Natl. Acad. Sci. U. S. A.* **2013**, *110* (17), 6640−6645.
(206) Henzie, J.; Grünwald, M.; Widmer-Cooper, A.; Geissler, P. L.; Yang, P. Self-Assembly of Uniform Polyhedral Silver Nanocrystals into Densest Packings and Exotic Superlattices. *Nat. Mater.* **2012**, *11* (2), 131−137.
(207) Gao, B.; Arya, G.; Tao, A. R. Self-Orienting Nanocubes for the Assembly of Plasmonic Nanojunctions. *Nat. Nanotechnol.* **2012**, *7* (7), 433−437.
(208) An, C.; Wang, R.; Wang, S.; Zhang, X. Converting Agcl Nanocubes to Sunlight-Driven Plasmonic Agcl: Ag Nanophotocatalyst with High Activity and Durability. *J. Mater. Chem.* **2011**, *21* (31), 11532−11536.
(209) Yang, C.; Wong, C. P.; Yuen, M. M. Printed Electrically Conductive Composites: Conductive Filler Designs and Surface Engineering. *J. Mater. Chem. C* **2013**, *1* (26), 4052−4069.
(210) Wu, B.; Heidelberg, A.; Boland, J. J. Mechanical Properties of Ultrahigh-Strength Gold Nanowires. *Nat. Mater.* **2005**, *4* (7), 525−529.
(211) Sun, J.; He, L.; Lo, Y.-C.; Xu, T.; Bi, H.; Sun, L.; Zhang, Z.; Mao, S. X.; Li, J. Liquid-Like Pseudoelasticity of Sub-10-Nm Crystalline Silver Particles. *Nat. Mater.* **2014**, *13* (11), 1007−1012.
(212) Dou, R.; Xu, B.; Derby, B. High-Strength Nanoporous Silver Produced by Inkjet Printing. *Scr. Mater.* **2010**, *63* (3), 308−311.
(213) Peng, P.; He, P.; Zou, G.; Liu, L.; Zhou, Y. N. Interfacial Nano-Mechanical Properties of Copper Joints Bonded with Silver Nanopaste near Room Temperature. *Mater. Trans.* **2015**, *56* (7), MI201412 DOI: 10.2320/matertrans.MI201412.
(214) Grouchko, M.; Roitman, P.; Zhu, X.; Popov, I.; Kamyshny, A.; Su, H.; Magdassi, S. Merging of Metal Nanoparticles Driven by Selective Wettability of Silver Nanostructures. *Nat. Commun.* **2014**, *5*, 2994 DOI: 10.1038/ncomms3994.
(215) Marzbanrad, E.; Rivers, G.; Peng, P.; Zhao, B.; Zhou, N. Y. How Morphology and Surface Crystal Texture Affect Thermal Stability of a Metallic Nanoparticle: The Case of Silver Nanobelts and Pentagonal Silver Nanowires. *Phys. Chem. Chem. Phys.* **2015**, *17* (1), 315−324.
(216) Wu, C.-D.; Fang, T.-H.; Wu, C.-C. Atomistic Simulations of Nanowelding of Single-Crystal and Amorphous Gold Nanowires. *J. Appl. Phys.* **2015**, *117* (1), 014307.

DOI: 10.1021/acsami.5b02134
ACS Appl. Mater. Interfaces 2015, 7, 12597−12618